AD-A094 137 ROME AIR DEVELOPMENT CENTER GRIFFISS AFB NY F/G 17/9
ESTIMATION OF THE ZONE OF DETECTION OF THE SINGLE WIRE INDIVIDU--ETC(U)
AUG 80 J L POIRIER
UNCLASSIFIED RADC-TR-80-258 NL

END
DATE FILMED
2-81
DTIC

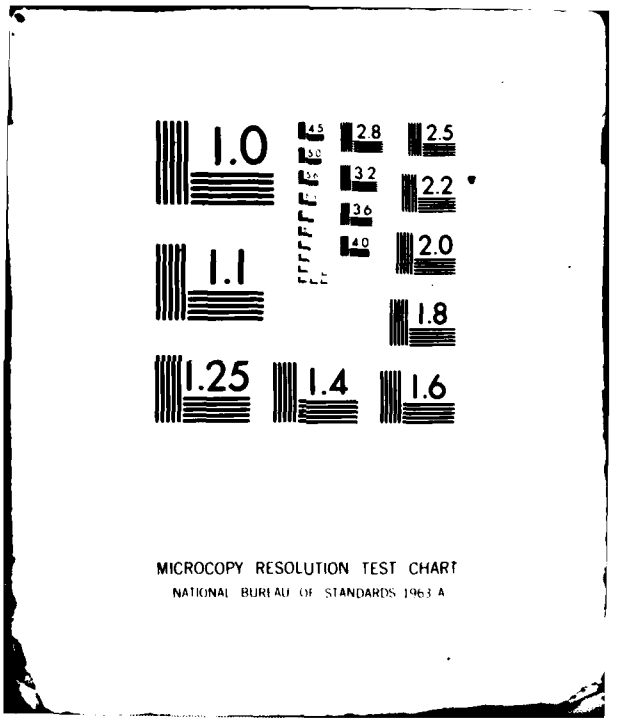
1.0
1.1
1.25
1.4
1.6
1.8
2.0
2.2
2.5
2.8
3.2
3.6
4.0
MICROCOPY RESOLUTION TEST CHART
NATIONAL BUREAU OF STANDARDS 1963 A

Unclassified

SECURITY CLASSIFICATION OF THIS PAGE (When Data Entered)

REPORT DOCUMENTATION PAGE	READ INSTRUCTIONS BEFORE COMPLETING FORM
1. REPORT NUMBER: RADC-TR-80-258	2. GOVT ACCESSION NO.: AD-A094234	3. RECIPIENT'S CATALOG NUMBER
4. TITLE (and Subtitle): ESTIMATION OF THE ZONE OF DETECTION OF THE SINGLE WIRE INDIVIDUAL RESOURCE PROTECTION SENSOR	5. TYPE OF REPORT & PERIOD COVERED: In-House
	6. PERFORMING ORG. REPORT NUMBER
7. AUTHOR(s): J. Leon Poirier	8. CONTRACT OR GRANT NUMBER(s): Technical Reports
9. PERFORMING ORGANIZATION NAME AND ADDRESS: Deputy for Electronic Technology (RADC/EEC) Hanscom AFB Massachusetts 01731	10. PROGRAM ELEMENT, PROJECT, TASK AREA & WORK UNIT NUMBERS: 61102F 23053408 J4
11. CONTROLLING OFFICE NAME AND ADDRESS: Deputy for Electronic Technology (RADC/EEC) Hanscom AFB Massachusetts 01731	12. REPORT DATE: August 1980
	13. NUMBER OF PAGES: 48
14. MONITORING AGENCY NAME & ADDRESS (if different from Controlling Office)	15. SECURITY CLASS. (of this report): Unclassified
	15a. DECLASSIFICATION DOWNGRADING SCHEDULE

16. DISTRIBUTION STATEMENT (of this Report)

Approved for public release; distribution unlimited.

17. DISTRIBUTION STATEMENT (of the abstract entered in Block 20, if different from Report)

18. SUPPLEMENTARY NOTES

19. KEY WORDS (Continue on reverse side if necessary and identify by block number)

Intrusion detection
Radio frequency intrusion sensor
Surface wave sensor
SWIRPS
IRPS

20. ABSTRACT (Continue on reverse side if necessary and identify by block number)

The response of an RF intrusion detection system which makes use of a leaky coaxial cable sensor is analyzed. The system consists of a length of leaky cable encircling the protected resource, which acts as a distributed transmitting sensor. A centrally-located monopole serves as a receiving element. When an intruder approaches the leaky cable sensor, the field is disturbed, the received signal changes, and if the change is sufficiently large, a detection is declared. It is shown that for most system applications the -

DD FORM 1 JAN 73 1473 EDITION OF 1 NOV 65 IS OBSOLETE

Unclassified

SECURITY CLASSIFICATION OF THIS PAGE (When Data Entered)

309050

20. Abstract (Continued)

amplitude of the signal scattered out of the leaky coaxial cable field by the intruder may be assumed to vary inversely with the distance of the intruder from the cable. The responses of the system with this field variation assumed are computed for several intrusion paths and agree well with observations. The probability of detection $P_D^{\square}$ and zone of containment $Z_C^{\square}$ are calculated for two receivers, one with an envelope detector and another with a quadrature detector. The uniformity of the $P_D^{\square}$ and $Z_C^{\square}$ along the cable are examined as a function of the cable constants. It is shown that optimal performance is obtained with a leaky cable sensor whose coupling coefficient is increased along the sensor to compensate for the loss in signal due to cable attenuation.

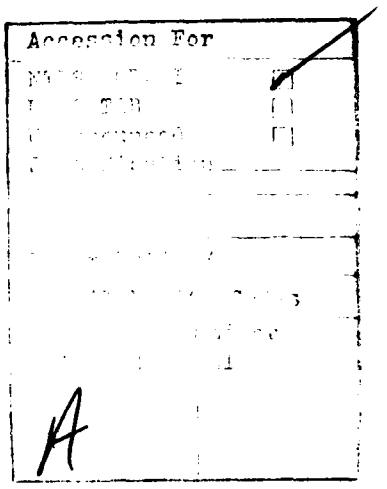

Contents

Illustrations

Illustrations

Estimation of the Zone of Detection of the Single Wire Individual Resource Protection Sensor

1. INTRODUCTION

In two previous reports,[1,2] the response of an RF intrusion system, which makes use of a leaky coaxial cable sensor, was analyzed. These analyses involved the computation of the variation of the received power as an intruder moved along the sensor cable, and gave an estimate of the detection sensitivity of the sensor. The present analysis considers the response to an intruder moving away from the cable sensor, and thus allows the computation of the zone of detection of such a system.

The elements of a basic system consist of a length of leaky cable, encircling the resource to be protected, which acts as a distributed transmitting sensor, and a centrally-located receiving antenna. When an intruder approaches the leaky cable sensor, the field is disturbed, the received signal changes, and, if the change is sufficiently large, a detection is declared. The layout of a basic system is shown in Figure 1. One end of the leaky coaxial cable is connected to a low-power transmitter and the other, terminated in a matched load. The receiving element is a monopole antenna. The received signal is processed by appropriate

(Received for publication 11 August 1980)

1. Poirier, J. L. and Kushner, M. (1978) Analysis of the Response of an RF Intruder Protection System, RADC-TR-78-17, AD A072 816.
2. Poirier, J. L. (1979) Effects of Multiple Receiving Antennas on the Response of an RF Intrusion Sensor, RADC-TR-79-42, AD A072 819.

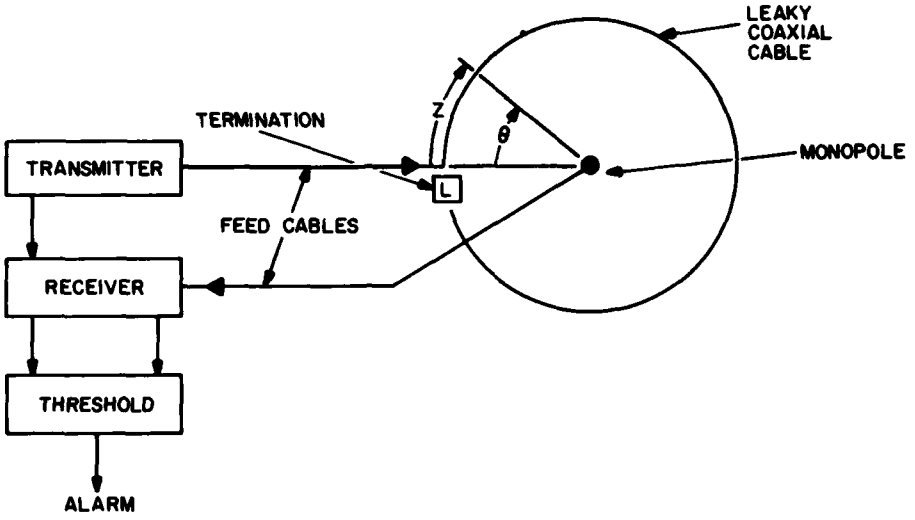

Figure 1. Elements of a Single Wire Individual Resource Protection Sensor

filters and thresholding circuits to maximize the detection sensitivity for human frame motion.

For these analyses, it was assumed that the only effect of the intruder was to scatter some energy out of the field set up in the vicinity of the leaky coaxial cable. This scattered energy propagated to the receiving antenna and added to the ambient field there. Thus, the antenna terminal voltage depended on the relative phase and amplitude of the scattered and ambient fields. The scattered field depended on the location of the intruder relative to the leaky cable and varied as the intruder moved. The field intensity near the leaky coaxial cable coax cable was represented by

$$v = v_o \left[e^{(-\alpha_1 - j\beta_1)z} + C_2 e^{(-\alpha_2 - j\beta_2)z} \right] e^{j\omega t} \qquad (1)$$

to account for the two modes which propagate on such a cable. The first term was associated with the coaxial (bifilar) mode, which has most of its power carried within the cable. The second term was associated with the surface attached (monofilar) mode, which has most of its energy propagating outside the cable. The constants α_1, β_1, and α_2, β_2 are the attenuation and phase constants for the two modes, ω is the angular frequency, and v_o and C_2 are constants which depend on the cable

characteristics and its environment. The total field at any point z along the cable is thus made up of a contribution from each of these modes. The surface-attached mode is very sensitive to the medium external to the cable and interacts strongly with objects near the cable. In contrast, the coaxial mode propagation is little affected by the properties of the medium into which the cable is placed.

The phase and amplitude of the energy scattered by an intruder at a point z adjacent to the cable was assumed proportional to that of the field there as represented by Eq. (1). With this assumption, the variation in received power as an intruder walked along the cable was computed and found to be in good agreement with measurements. In the present case, however, Eq. (1) must be modified to show the radial dependence of the fields, so that the response of the system as an intruder moves away from the cable may also be computed.

In the following sections, a phenomenological model which describes the radial decay of the leaky coaxial cable fields will be developed and used to compute the response of the Single Wire Individual Resource Protection Sensor (SWIRPS) to an intruder as he moves in the region near the sensor cable. The calculations will focus on radial paths and the rate of decay in the response with distance from the cable along these paths. The output of a receiver with an envelope detector and one with a quadrature detector will then be analyzed. This will serve as the basis for computing the probability of detection P_D and the zone of containment Z_C, where detections provided by the SWIRPS can occur.

2. FIELD DISTRIBUTION

A simple model for the variation of the fields around a leaky coaxial cable is adequate for the present purpose, therefore no attempt will be made to describe the precise nature of the interaction of the intruder with the sensor fields. Instead, a reasonable distribution for the external leaky cable fields, based on theoretical considerations and existing experimental data, will be developed. The validity of the model will be demonstrated by comparing the results of measurements on SWIRPS with predicted values.

In this analysis, the cable is assumed to be on the surface of the ground (Figure 2); however, measurements have shown that there is little difference in the character of the response when the cable is buried up to nine inches deep. It is further assumed that the cable is in a homogeneous medium (air) and that the presence of the earth-air interface does not significantly modify the relative system response.

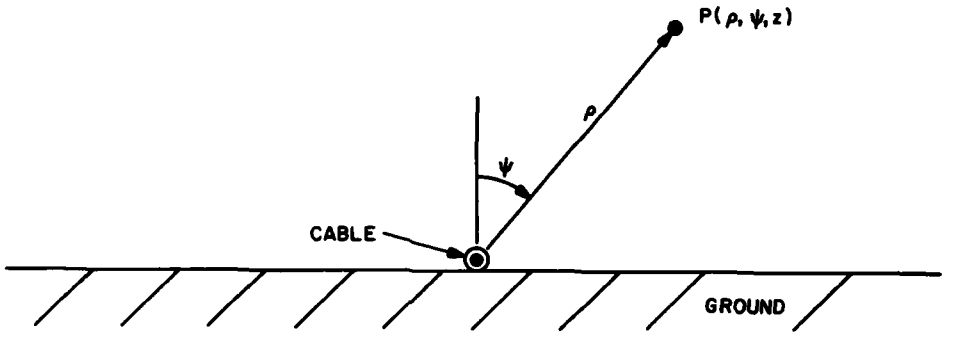

Figure 2. Cross Section Geometry

Rawat[3] applied a numerical technique to compute the propagation characteristics of coaxial cables in free space, with loosely braided outer sheaths and solid sheaths with closely-spaced slots. Fernandes[4] recently provided a closed form solution for lossless leaky cables based on the concept of surface transfer impedance used as Delogne[5] and Wait.[6] These results show the existence of a coaxial (bifilar) mode, as well as a surface attached (monofilar) mode as was discussed in connection with Eq. (1).

The expressions for the fields around a lossless leaky cable in free space obtained by Fernandes[4] are

$$E_z = K H_0^1(jh_o\rho)\, e^{-j(\beta z-\omega t)} \tag{2a}$$

$$E_\rho = K \frac{\beta}{h_o} H_1^1(jh_o\rho)\, e^{-j(\beta z-\omega t)} \tag{2b}$$

---

3. Rawat, V. (1973) Unorthodox Transmission Lines for Continuous Access Guided Communication (CAGC) PhD Thesis - Dept. of Electrical Eng., Queen's University, Kingston, Ontario, Canada.

4. Fernandes, A.S. de C. (1979) Propagation characteristics of a loose braid coaxial cable in free space, Radio and Electronic Eng., 49, No. 5, pp 255-260, May 1979.

5. Delogne, P.O. and Safak, M. (1975) Electromagnetic theory of the leaky coaxial cable, The Radio and Electronic Eng., 49, pp 233-40, May 1975.

6. Wait, J.R. and Hill, D.A. (1975) Propagation along a braided coaxial cable in a circular tunnel, IEEE Trans. on Microwave Theory and Techniques, MTT-23, No. 5, pp 401-5, May 1975.

$$H_\psi = K \frac{k_o^2}{\omega \mu_o h_o} H_1^1(jh_o\rho)\, e^{-j(\beta z - \omega t)} \qquad (2c)$$

where K is a constant, H_0^1 and H_1^1 are zero and first order Hankel functions of the first kind respectively, ω the angular frequency of the impressed signal, β the longitudinal wave number, k_o the free space wave number, $h_o = [\beta^2 - k_o^2]^{1/2}$ the transverse wave number, and z the longitudinal distance from the cable input. Equations (2a–c) describe both the mono- and bifilar modes, depending on the value inserted for the propagation constant β.

Fernandes[4] obtained expressions for $\beta = \beta_1$ and $\beta = \beta_2$ appropriate for the coaxial and surface attached modes respectively, in terms of an equivalent sheath inductance and other cable construction parameters. In the present analysis, the values for β_1 and β_2 will be deduced from measurements of the interference between the ambient and scattered fields at the receiving antenna. Generally, $\beta_1 \approx k_o\sqrt{\varepsilon_r}$, and this mode is most affected by the relative dielectric constant ε_r of the material inside the cable where most of its energy is confined. In contrast, β_2 is generally less than β_1, and most of the energy associated with this mode is outside the cable.

The power density at any point outside the cable computed from the expressions in Eqs. (2a–c) is found to be

$$P_z = \frac{K^2 \beta k_o^2}{2\omega\mu_o[\beta^2 - k_o^2]} [H_1^1(j[\beta^2 - k_o^2]^{1/2}\rho)]^2 \qquad (3)$$

where β_1 or β_2 can be inserted for β to obtain P for the corresponding mode. A straightforward application of a polynomial representation[7] for the Hankel function gives the radial decay in P_z, plotted in Figure 3. Comparison of the two solid curves clearly shows the greater radial extent of the fields associated with the monofilar mode, and illustrates the reason for its greater sensitivity to external conditions. Comparison of the power density variation for the two modes with a $1/\rho^2$ decay (represented by the dashed line) shows that near the cable, each curve falls off at about the same rate as expected. Only when ρ becomes sufficiently large does the exponential decay associated with the Hankel function become evident.

Inspection of Figure 3 shows that measurements of the power density around leaky cables could appear to follow a $1/\rho^2$ law unless they were carried out to

7. Ambramowitz, M. (1964) Handbook of Mathematical Functions, N. Bur. of Stnd., U.S. Printing Office, Washington, D.C.

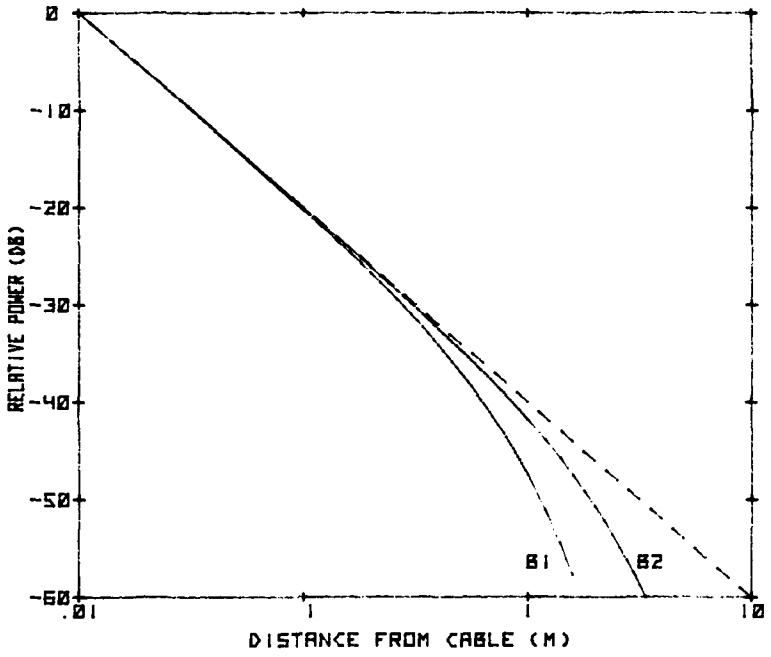

Figure 3. Variation in Power Density with Distance from a Lossless Cable. $\alpha_1 = \alpha_2 = 0$, $\beta_1 = 2.15$ rad/m, $\beta_2 = 1.65$ rad/m

sufficiently large distances. Cree and Giles[8] and Yoh, et al,[9] measured the radial falloff of power and found it to be approximately $1/\rho^2$. However, the former observed this decay rate no matter how far away from the cable the field was probed. Perhaps, some of the bound wave energy was converted into a radiating mode by small discontinuities in the cable and surrounding environment.

To examine the variation of the phase of the fields around the cable, a more general solution to the axial surface waves associated with the cables must be developed. Inspection of Eqs. (2a–c) shows that there is no variation in phase as ρ increases because h_o, the transverse wave number, is real. This result is a consequence of the assumption of a lossless system. If, instead, the longitudinal propagation factor is taken to be $\gamma = \alpha + j\beta$, then the transverse wave number would

8. Cree, D.J. and Giles, L.J. (1975) Practical performance of radiating cables, REE, Vol. 45, No. 5, pp 221-223, May 1975.

9. Yoh, P., Esposito, R., Gagnon, R., and Kodis, R.D. (1974) Measurements of Leaky Coaxial Cables and Possible Applications to Train Communications, Report No. FRA-ORD & D-74-43, U.S. Department of Transportation, May 1974.

become $h_o = [-(\gamma^2 + k_o^2)]^{1/2}$ and would have both a real and an imaginary part. The imaginary part of h_o would produce a shift in the phase of the fields as ρ increases and would cause the equiphase surfaces to tilt forward.

The evaluation of the modulus and phase of the expressions[10]

$$E_z = K H_0^1(jh_o\rho)\, e^{(-\alpha-j\beta)z+j\omega t} \tag{4a}$$

$$E_\rho = K \frac{\gamma}{jh_o} H_1^1(jh_o\rho)\, e^{(-\alpha-j\beta)z+j\omega t} \tag{4b}$$

$$H_\psi = K \frac{\omega \varepsilon_o}{h_o} H_1^1(jh_o\rho)\, e^{(-\alpha-j\beta)z+j\omega t} \tag{4c}$$

for the fields when h_o is complex is not easily carried out. However, the formal insertion of the complex argument into the power series representation for the Hankle functions can be used to evaluate Eqs. (4a–c).

The transverse wave number can be written in terms of its real and imaginary parts as

$$h_o = h_r + jh_i \tag{5}$$

where

$$h_r = [(\beta^2 - \alpha^2 - k_o^2)^2 + 4\alpha^2\beta^2]^{1/4} \cos\left[1/2 \tan^{-1}\left(\frac{2\alpha\beta}{\alpha^2 + k_o^2 - \beta^2}\right)\right] \tag{6}$$

and

$$h_i = [(\beta^2 - \alpha^2 - k_o^2)^2 + 4\alpha^2\beta^2]^{1/4} \sin\left[1/2 \tan^{-1}\left(\frac{2\alpha\beta}{\alpha^2 + k_o^2 - \beta^2}\right)\right] . \tag{7}$$

Typical values for the phase and attenuation factors (f = 75 MHz) in Eqs. (6) and (7) are $\alpha = 0.0075$ n/m, $\beta = 2.2$ rad/m, $k_o = 1.57$ rad/m. Thus $h_r = 2.38\ m^{-1}$ and $h_i = 0.02\ m^{-1}$, $h_o \approx h_r$, and the equiphase surfaces are very nearly

10. Barlow, H.M. and Brown, J. (1962) Radio Surface Waves, International Monographs on Radio, Oxford at the Clarendon Press.

perpendicular to the cable. This has in fact been observed in a series of careful measurements.[11]

In view of the above discussion, the radial component of the electric field can be written as

$$E_\rho \approx K_n \frac{e^{(-\alpha_n - j\beta_n)z + j\omega t}}{\rho} \tag{8}$$

where n = 1 or 2 to represent the bifilar or monofilar modes respectively. With $K_1 = v_o \rho_o$ and $K_2 = v_o C_2 \rho_o$, Eq. (1) may be modified to account for the field away from the cable by simply inserting a $1/\rho$ dependence into each term. Thus

$$v = \frac{v_o \rho_o}{\rho} \left\{ e^{(-\alpha_1 - j\beta_1)z} + C_2 e^{(-\alpha_2 - j\beta_2)z} \right\} e^{j\omega t} , \tag{9}$$

where ρ_o is a normalizing factor to make Eq. (9) reduce to the form of Eq. (1) when $\rho = \rho_o$.

3. *VARIATION IN RECEIVED POWER*

For the purpose of these calculations, it is assumed that the principal effect of the intruder is to scatter some energy out of the field surrounding the leaky coax cable. The scattered field produces a voltage V_I at the terminals of the receiving antenna, represented by

$$V_I = AP\,v \tag{10}$$

where A accounts for the scattering amplitude of the intruder and the gain of the receiving antenna, and P describes the propagation of the scattered field from the intruder to the antenna.

The propagation factor appropriate for a single centrally-located receiving antenna is set equal to

$$P = \frac{r_o e^{-j\beta_3 (r - r_o)}}{r} \tag{11}$$

---

11. Harman, K. (1979) private communication.

where r_o is the distance from the intruder at the cable and the antenna, r is the distance from the intruder anywhere along the radial path and the antenna, and β_3 is the free space phase constant.

In the absence of an intruder, a voltage of the form

$$V = Be^{j\phi} \tag{12}$$

is present at the antenna terminals. The amplitude and phase of this voltage can be related to the operating frequency, cable properties, and geometry of the system. The total voltage developed in the presence of an intruder is

$$V_T = V + V_I \ . \tag{13}$$

and the total power is thus proportional to

$$V_T V_T^* = VV^* + 2Re\ VV_I^* + V_I V_I^* \tag{14}$$

where the * denotes the complex conjugate and Re means the real part of VV_I^*. The relative received power is then defined as

$$P_Q = 10 \log \left(\frac{V_T V_T^*}{V V^*} \right) \ , \tag{15}$$

the quantity measured in the authors experiments.

3.1 Sensor Response for Radial Crossings

The expression for $V_T V_T^*$ which results from these equations is found to be

$$V_T V_T^* = B^2 + \frac{2|A|B\rho_o r_o |v_o|}{\rho r} \left\{ e^{-\alpha_1 z} \cos [\phi - \delta + \alpha + \beta_1 z + \beta_3 (r - r_o)] + |C_2|\, e^{-\alpha_2 z} \cos [\phi - \delta - \zeta + \alpha + \beta_2 z + \beta_3 (r - r_o)] \right\}$$

$$+ \frac{\rho_o^2 r_o^2 |v_o|^2 |A|^2}{\rho^2 r^2} \left\{ e^{-2\alpha z} + 2 |C_2| e^{(-\alpha_1 - \alpha_2)z} \cos [\zeta + (\beta_1 - \beta_2)z] \right.$$

$$\left. + |C_2|^2 e^{-2\alpha_2 z} \right\} \tag{16}$$

where δ, α, and ζ are the angles associated with v_o, A, and C_2 respectively. The first term of this equation is recognized as proportional to the ambient power, and the last term to the power scattered by the intruder. The cross term gives rise to the interference observed when an intruder enters the zone of detection.

The relationship between the various variables and normalizing factors which appear in Eq. (16) is shown in Figure 4. The distance from the cable to the intruder measured along the ground is represented by x. It is assumed that the intruder has an effective scattering center a distance y above the ground. Values of y ranging from about 0.2 to 0.6 m give reasonable results. Thus from Figure 4:

$$r = [(R_o + x)^2 + y^2]^{1/2} \tag{17a}$$

$$\rho = [x^2 + y^2]^{1/2} \tag{17b}$$

$$r_o = [R_o^2 + y^2]^{1/2} \tag{17c}$$

$\rho_o = y$, and R_o is the radius of the loop.

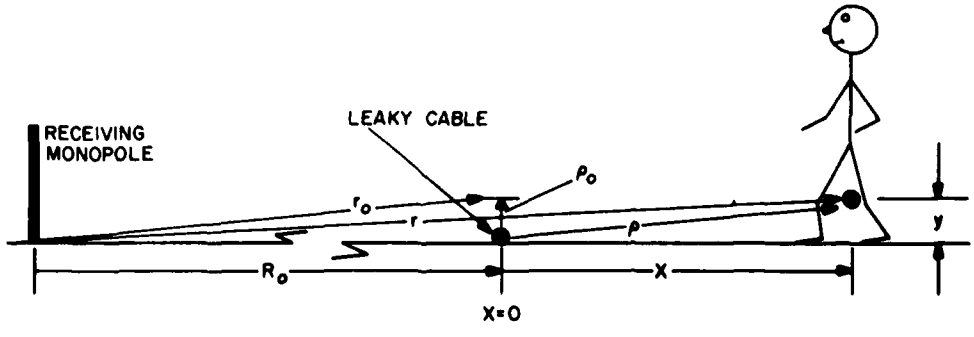

Figure 4. Geometrical Relationship Among System Variables

The received power P_Q is plotted in Figure 5 for a radial path that intersects the cable at z_o = 50 m from the input of a 152-m cable. The amplitude of the response decreases rapidly with the distance x because of the dropoff of the field around the leaky coax cable. Inspection of Figure 5 shows that the peak response does not occur when intruder is at the cable. The position of the peak depends on the relative phase of V_I and V at x 0. This is a function of the azimuth of the radial path. This behavior is illustrated by the curves shown in Figure 6. These curves represent the responses along seven adjacent radial paths spaced about 1 m apart at the cable. The azimuth of the center path is located by the distance z_o; this path serves as the reference for the set. The response for the reference radial of Figure 6 is the same as that shown in Figure 5. The shift in the location and intensity of the maximum response from one path to the other is evident

The variation in received power observed in an experiment is shown in Figure 7(a). The shift in the location of the peak is evident, as is the rapid dropoff in the response as the intruder moves away from the cable. The calculated responses for the same set of radials are plotted in Figure 7(b), and show excellent agreement with the measurements.

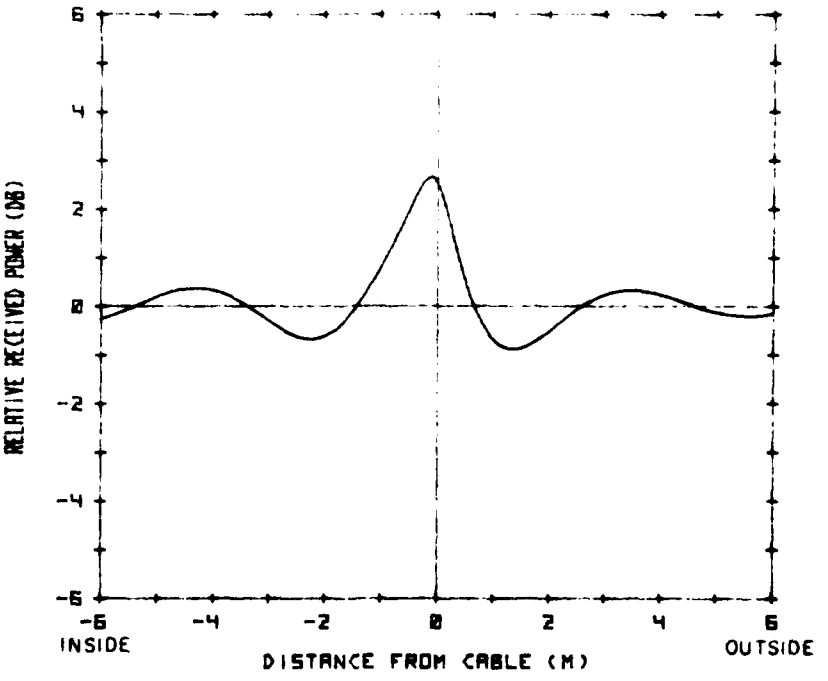

Figure 5. Computed Variation of Received Power as an Intruder Moves Along a Radial Path. $\gamma_1 = 0.0075 + j\,2.15\ m^{-1}$, $\gamma_2 = 0.01 + j\,1.65\ m^{-1}$, z_o = 50 m, L = 152 m, y = 0.4 m

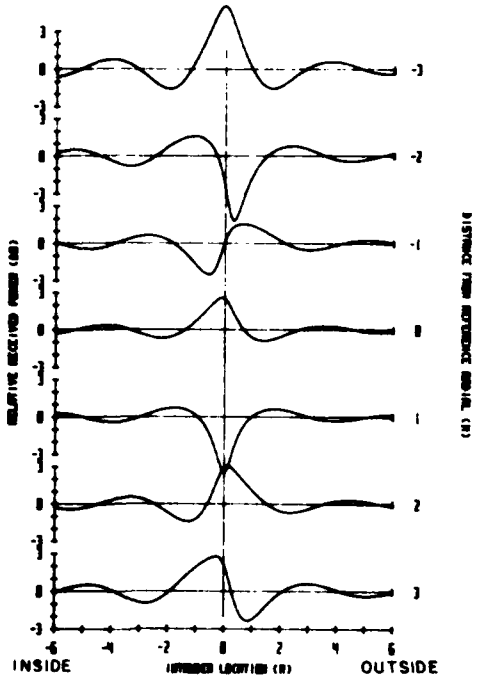

Figure 6. Computed Responses for Several Adjacent Radial Intrusion Paths. $\gamma_1 = 0.0075 + j\,2.15\ m^{-1}$, $\gamma_2 = 0.01 + j\,1.65\ m^{-1}$, $z_o = 50$ m, L = 152 m, y = 0.4 m

It is important in any intrusion system to maintain a uniform sensitivity of detection around the perimeter of the loop. In this system, the principal cause of the decrease in the detection sensitivity is the attenuation of the signal as it propagates along the leaky coax cable. To display the effect of this on the sensitivity and the radial extent of the detection zone, Eq. (16) was evaluated near the three additional azimuths of 2, 100, and 150 m. The results are plotted in Figure 8. It is immediately evident from Figure 8(a) that a significant variation in received power is produced by an intruder, even while several meters from the sensor, when his radial path is near the cable input. The extent of the variation does, however, also depend on the relative magnitude of the intruder and ambient signals. Figures 8(b) and 8(c) show that further along the cable, the radial extent of the response as well as its maximum value are diminished because the cable attenuation reduces the intensity of the leakage field near the cable. The slow variation in the amplitude of the peak as one moves from azimuth to azimuth is due to the interaction of the surface wave and inner coaxial wave components interfering

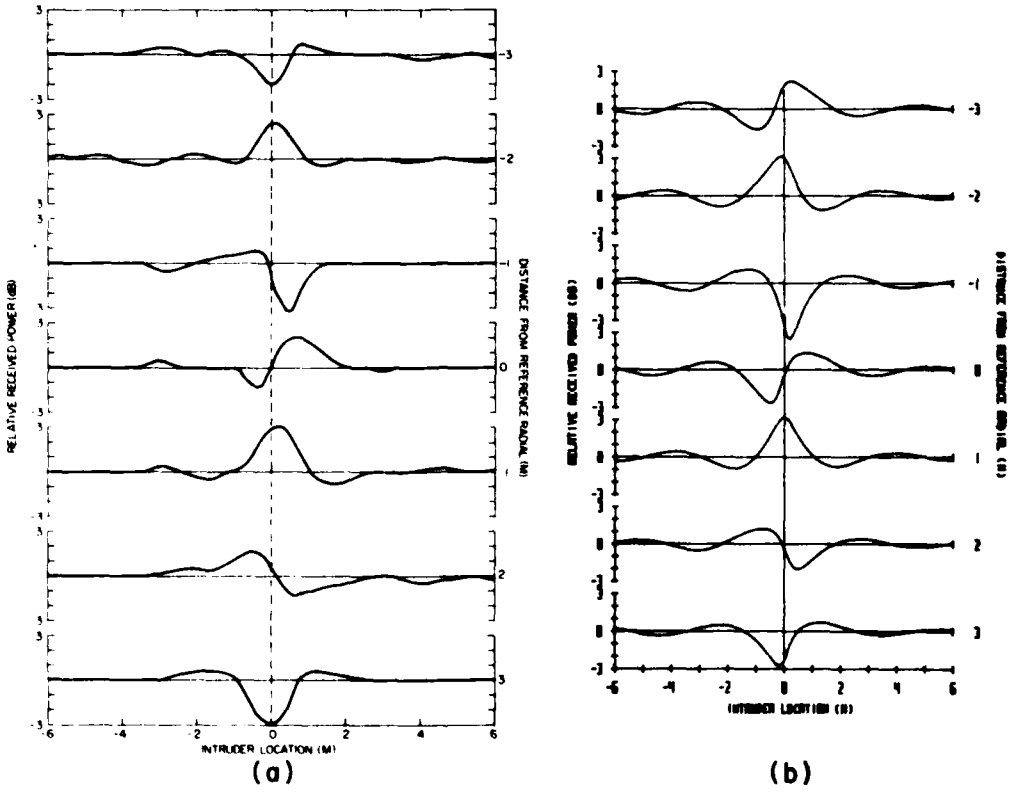

Figure 7. Responses for Several Radial Intrusion Paths. z_o = 130 m, y = 0.4 m, L = 152 m. (a) Observed, (b) Computed: γ_1 = 0.0075 + j 2.15 m^{-1}, γ_2 = 0.01 + j 1.65 m^{-1}

along the cable. This effect tends to die out with distance along the cable if the surface wave attenuation is greater than that for the coaxial mode.

In the next section, the response of the system for an intruder walking around the perimeter of the sensor cable will be shown. These circumferential path responses offer a convenient way of evaluating the effects of modifying various system parameters.

3.2 Sensor Response for Circumferential Paths

Equation (16) can be evaluated for a circumferential path at any distance x from the cable sensor. The results for x = o m are shown in Figure 9. The fast oscillations are produced because phase of the intruder changes as he walks around the cable, thus setting up an interference pattern between the ambient and intruder signals. The amplitude of the oscillations depends on the ratio of the ambient and

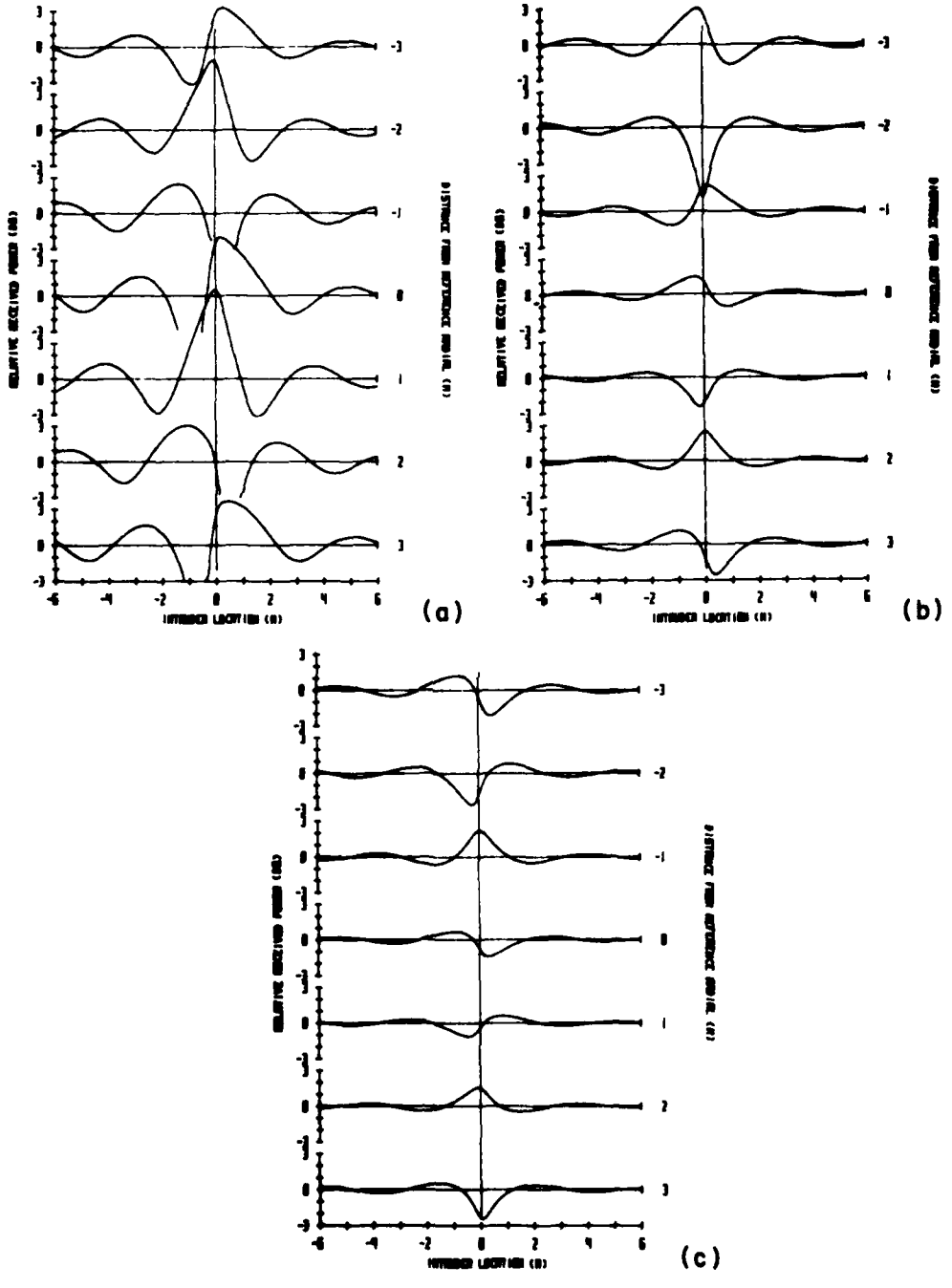

Figure 8. Computed Responses for Several Adjacent Radial Intrusion Paths at Three Distances from the Cable Input. $\gamma_1 = 0.0075 + j\,2.15\ m^{-1}$, $\gamma_2 = 0.01 + j\,1.65\ m^{-1}$, L = 152 m, y = 0.4 m. (a) z_o = 2 m, (b) z_o = 100 m, (c) z_o = 150 m

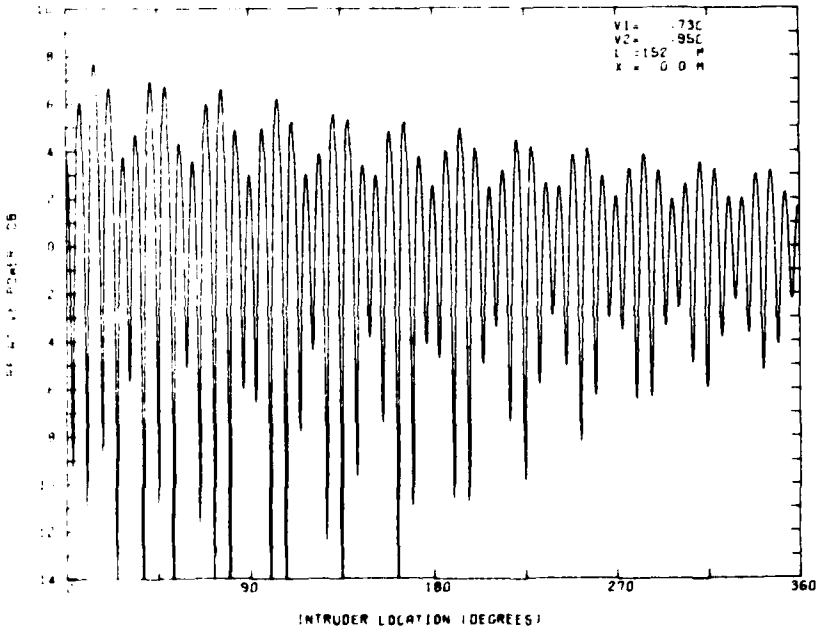

Figure 9. Computed Variation in Received Power for a Circumferential Path, $\gamma_1 = 0.0075 + j\,2.15\ m^{-1}$, $\gamma_2 = 0.01 + j\,1.65\ m^{-1}$, $y = 0.4$ m

intruder signals, and tends to decrease with distance along the cable. This is a result of the cable attenuation, which gradually causes the field strength along the cable and thus the intruder's signal to decrease. The slow variation in the response is a result of the interaction between the outer and inner waves. The degree of this interaction depends on the ratio of the surface to coaxial wave energy and the relative attenuation constants of the two waves. The period of these can be observed to be the effective phase constant $\beta = \beta_2 - \beta_1$.

The measured circumferential response is shown in Figure 10 and shows all the features discussed in connection with the computed values. The fine structure which can be seen near the peak of each cycle is a result of the motion of the intruder's arms and legs, which tends to modulate his scattering amplitude.

The responses for a number of circumferential paths at various distances from the cable are plotted in Figure 11 and show the expected rapid decrease in amplitude as the distance from the cable increases.

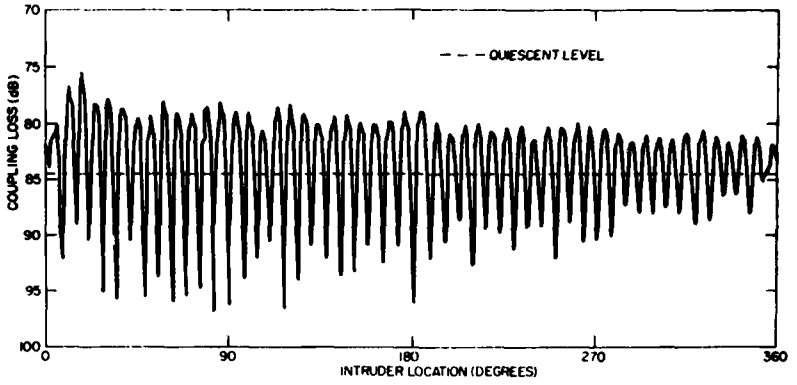

Figure 10. Variation in Received Power Observed in an Experiment for a Circumferential Path. L = 152 m, x = 0 m

3.3 Sensor Cable Propagation Constants

Some of the propagation constants are specified by the cable manufacturers, while others must be measured because they depend on the environment in which the cable is placed. In fact, the propagation constants can even be a function of position along the cable in sensors where the size of the holes in the sheath is gradually increased, to compensate for attenuation losses, in order to maintain a more uniform external field.[12]

The attenuation constant α_1 and the phase constant β_1 are always specified in the manufacturers data sheets and are easy to measure. The attenuation constant may be obtained by measuring the ratio of the cable output to input powers. At 75 MHz, the value for α_1 ranges from about 0.002 n/m to 0.01 n/m and increases with frequency, sheath hole size, and the dielectric constant and conductivity of the medium in which the cable is placed. The dielectric constant of the material inside the cable is the chief factor affecting the value of β_1. Solid or foam polyethelene with relative dielectric constants ranging from 2.1 to 1.5 are often used. This results in a phase constant $\beta_1 \approx k\sqrt{\varepsilon_r}$ in the range of 2.3 rad/m to 1.9 rad/m.

A plot of the response such as that shown in Figure 10 can also be used to estimate the values for α_1, and β_1, in this case, appropriate for the 152.4-m CERT-285[13] cable used in the experiment. Smoothing the slow variations of that curve to eliminate the effect of the mode interaction shows a drop of about 3.8 dB in the amplitude of the response from one end of the cable to the other. The peak

12. Poirier, J. Leon (1979) An Evaluation of Some Factors Affecting the Choice of Operating Frequency of a Guided Wave Radar for Intruder Detection, RADC-TR-79-83, AD A073 078.

13. Technical Memo 49, Revision No. 1, Times Wire and Cable Co., Wallingford, CT.

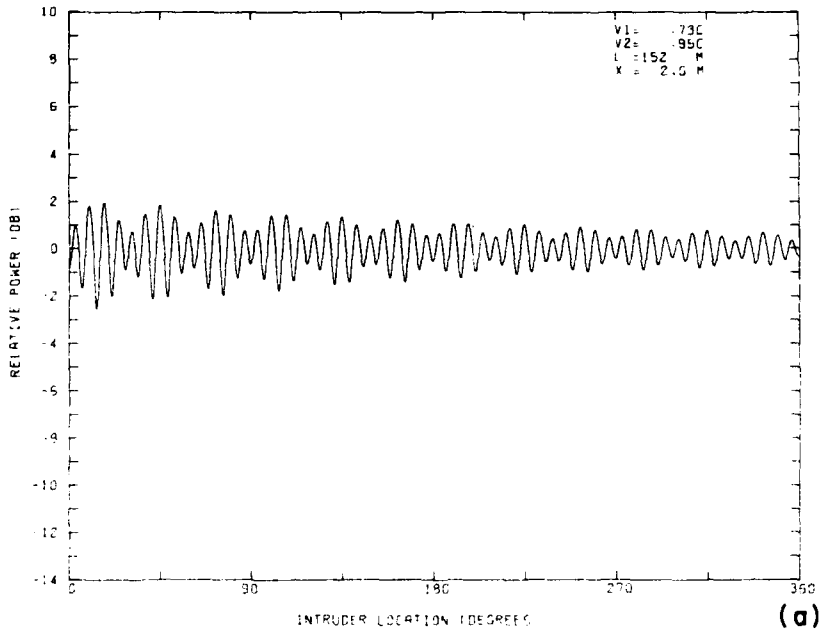

Figure 11. Computed Received Power Variation for a Number of Circumferential Paths. $\gamma_1 = 0.0075 + j\,2.15\ m^{-1}$, $\gamma_2 = 0.01 + j\,1.65\ m^{-1}$, y = 0.4 m

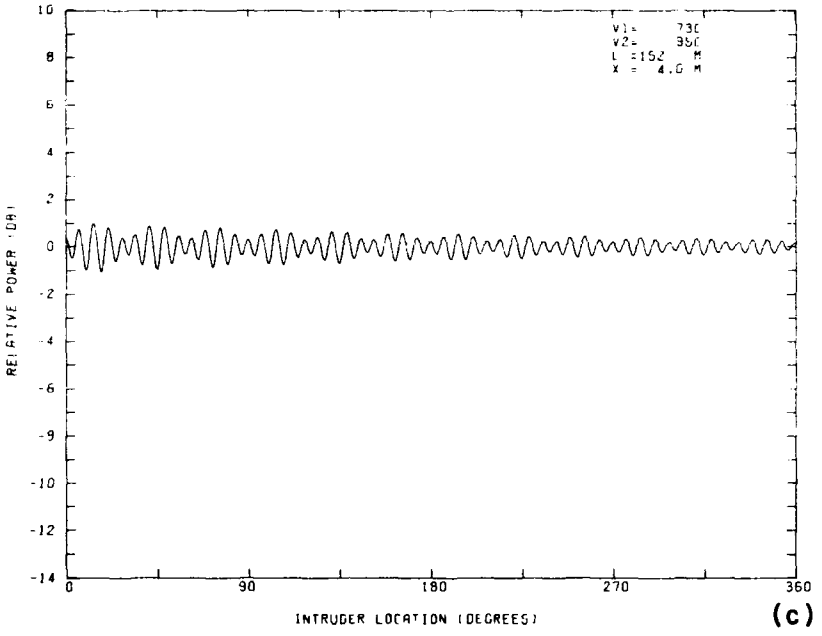

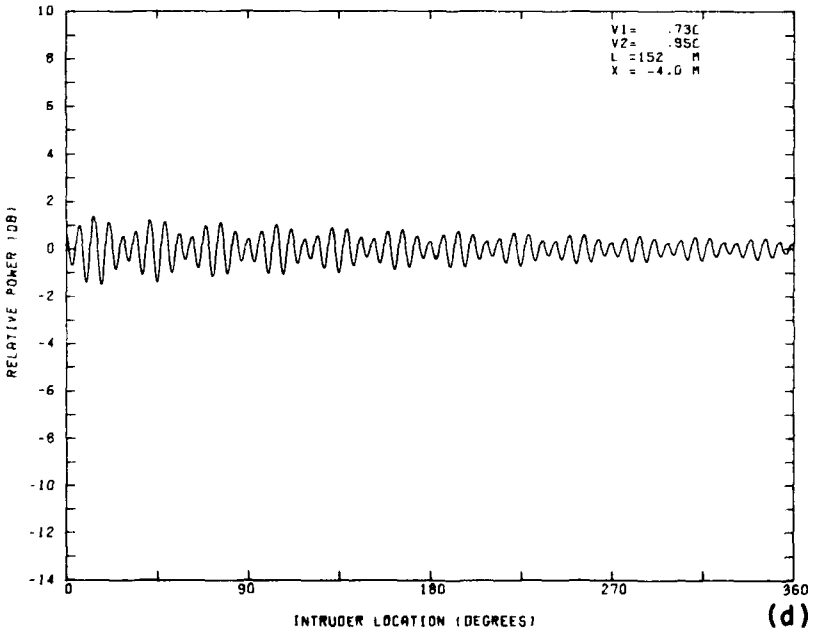

Figure 11. Computed Received Power Variation for a Number of Circumferential Paths. $\gamma_1 = 0.0075 + j\,2.15\ m^{-1}$, $\gamma_2 = 0.01 + j\,1.65\ m^{-1}$, $y = 0.4$ m (Cont.)

value of the response at the input is from the interference law for two coherent signals

$$P = P_A + P_I + 2\,(P_A P_I)^{1/2} \quad , \tag{18}$$

and at the termination end

$$P' = P_A + P_I' + 2\,(P_A P_I')^{1/2} \tag{19}$$

where P_A and P_I are the ambient and intruder induced, powers respectively. The intruder power P_I' at the far end is to a first approximation, related to P_I by

$$P_I' = P_I\, e^{-2\alpha L} \quad . \tag{20}$$

The ratio of P to P_A is from Figure 10 found to be about 6.3 dB, so that from Eq. (18)

$$P_I = 1.1\, P_A \quad . \tag{21}$$

Using this with Eqs. (18–20) and L = 152.4 m yields for the attenuation constant α = 0.0077 n/m. The value obtained by direct measurement was 0.0075 n/m.

The phase constant β_1 is obtained by counting the number of peaks N observed in the response along a segment of the cable. From Figure 10, N = 25.8 for the center half of the cable and from Eq. (16)

$$\beta_1 = 4\pi\, N/L = 2.14 \text{ rad/m} \quad . \tag{22}$$

The phase constant β_2 is obtained in a similar way by counting the number of peaks M in the slow variations of the amplitude. M ≈ 6.0 so that

$$\beta_2 = \beta_1 - 4\pi\, M/L = 1.65 \text{ rad/m} \quad . \tag{23}$$

The values for β_1 and β_2 correspond to propagation velocities of 0.73c and 0.95c, respectively, where c is the speed of light in vacuum.

To estimate the values for C_2 and α_2, Eq. (16) is applied to the curve of Figure 10 with $\rho = \rho_o$, $r = r_o$, and α_1 = 0.0076 n/m. As previously found (Eq. (21)), the intruder induced power (from the bifilar mode) is proporational to $|v_o|^2|A|^2 = 1.1\, B^2$ where B^2 is proportional to the ambient power. At the slow variation peak near 90^o, the total received power is proportional to

$$P_{MAX} = B^2 + 2|v_o||A|B\left\{e^{-\alpha_1 z} + |C_2|\, e^{-\alpha_2 z}\right\}$$

$$+ |v_o|^2|A|^2\left\{e^{-2\alpha_1 z} + 2|C_2|\, e^{(-\alpha_1-\alpha_2)z} + |C_2|^2\, e^{-2\alpha_2 z}\right\} \qquad (24)$$

where the angles ζ, α, and δ have been set to zero. At the next slow variation minimum,

$$P_{MIN} = B^2 + 2|v_o||A|B\left\{e^{-\alpha_1 z'} - |C_2|\, e^{-\alpha_2 z'}\right\}$$

$$+ |v_o|^2|A|^2\left\{e^{-2\alpha_1 z'} - 2|C_2|\, e^{(-\alpha_1-\alpha_2)z'} + |C_2|^2\, e^{-2\alpha_2 z'}\right\} \qquad (25)$$

where $z' = z + L/4M$. The distances z and z' in Eqs. (24) and (25) are each approximated by $z'' = (z + z')/2$ to facilitate the following computations. From Figure 10, $P_{MAX}/P_{MIN} = 2.8$ dB, which gives upon combining Eqs. (24) and (25)

$$|C_2|\, e^{-\alpha_2 z''} = 0.29 \ . \qquad (26)$$

Near 270°, $P_{MAX}/P_{MIN} = 1.2$ dB, $z''' = L(3 + 1/2M)/4$, and

$$|C_2|\, e^{-\alpha_2 z'''} = 0.12 \ . \qquad (27)$$

From these, $\alpha_2 = 0.01$ n/m and $|C_2| = 0.44$.

The attenuation constant α_2 depends on the properties of the medium near the cable. Experiments done with buried leaky coaxial cables have resulted in values for α_2 much larger than indicated for the present case in which the cable is placed on the surface of the ground. In fact, α_2 has been observed to change in response to the moisture content of the ground.

4. SYSTEM IMPLEMENTATION

The discussion of the response thus far has been in terms of the received power, or more precisely, in terms of the variation in coupling loss between the leaky coax cable and the receiving antenna. The analysis was cast in this format because this was the quantity which was measured in the laboratory experiments.

However, care must be taken when analyzing the performance of a system whose output is measured in terms of received power. The reason for this is that the amplitude of the observed oscillations in the received power depends on the intruder induced signal power relative to the ambient power. The amplitude is greatest when the two are equal. Thus the amplitude of the variations is not by itself an adequate measure of a system's performance. This effect can most easily be demonstrated by considering the interference law for two coherent signals

$$P = P_A + P_I + 2 (P_A P_I)^{1/2} \cos \Theta \quad . \tag{28}$$

The relative phase of the voltages which produce the terms proportional to the ambient and intruder powers, P_A and P_I respectively, is Θ. With this expression, $P_Q = 10 \log P$, was evaluated for three values of P_A.

The results for $P_A = P_I$ are shown in Figure 12(a). The ambient level is indicated by the horizontal line. The peak value is seen, as expected, to be 6 dB greater than ambient, and the minimum value is $-\infty$ dB since the curve is presented in terms of decibels. Figure 12(b) shows the curves for $P_I = 10P_A$ and $P_I = 0.1P_A$. The amplitudes of the variations are each diminished, but equal to one another. Thus an increase in intruder power can in fact cause the amplitude of the power variations to decrease. Of course, the peak value of the received power always increases in proportion to the intruder power.

The dependence of the amplitude of the response variations on the ambient power would not be of concern if the ambient power remained fixed at one level. However, the ambient power level is a sensitive function of environmental conditions. Another source of variation, particularly important for portable systems which are often moved from place to place, is the exact placement of the cable sensor and receiving antenna. Any variation in their relative placement would also cause the ambient power to differ. The ambient power is sensitive to system conditions because it results from the superposition of many voltage components from all parts of the cable. And thus, a change in the phase of one of the dominant components can cause a large change in the ambient power. The relative phases of the ambient components depend on the operating frequency, precise placement of the receiving antenna and sensor cable, and the environmental conditions. In contrast to the ambient power, the intruder's power depends principally on the field about the sensor cable; this is relatively insensitive to environmental conditions.

Therefore, when comparing the performance of two systems or that of one system at different times, the total received power variation relative to the ambient must be taken into account. Only then can the magnitude of the intruder's signal power be computed. Also, any system whose output response depends on the ambient power level requires a receiver-detector designed to accommodate changes in ambient conditions which could mask the presence of the intruder.

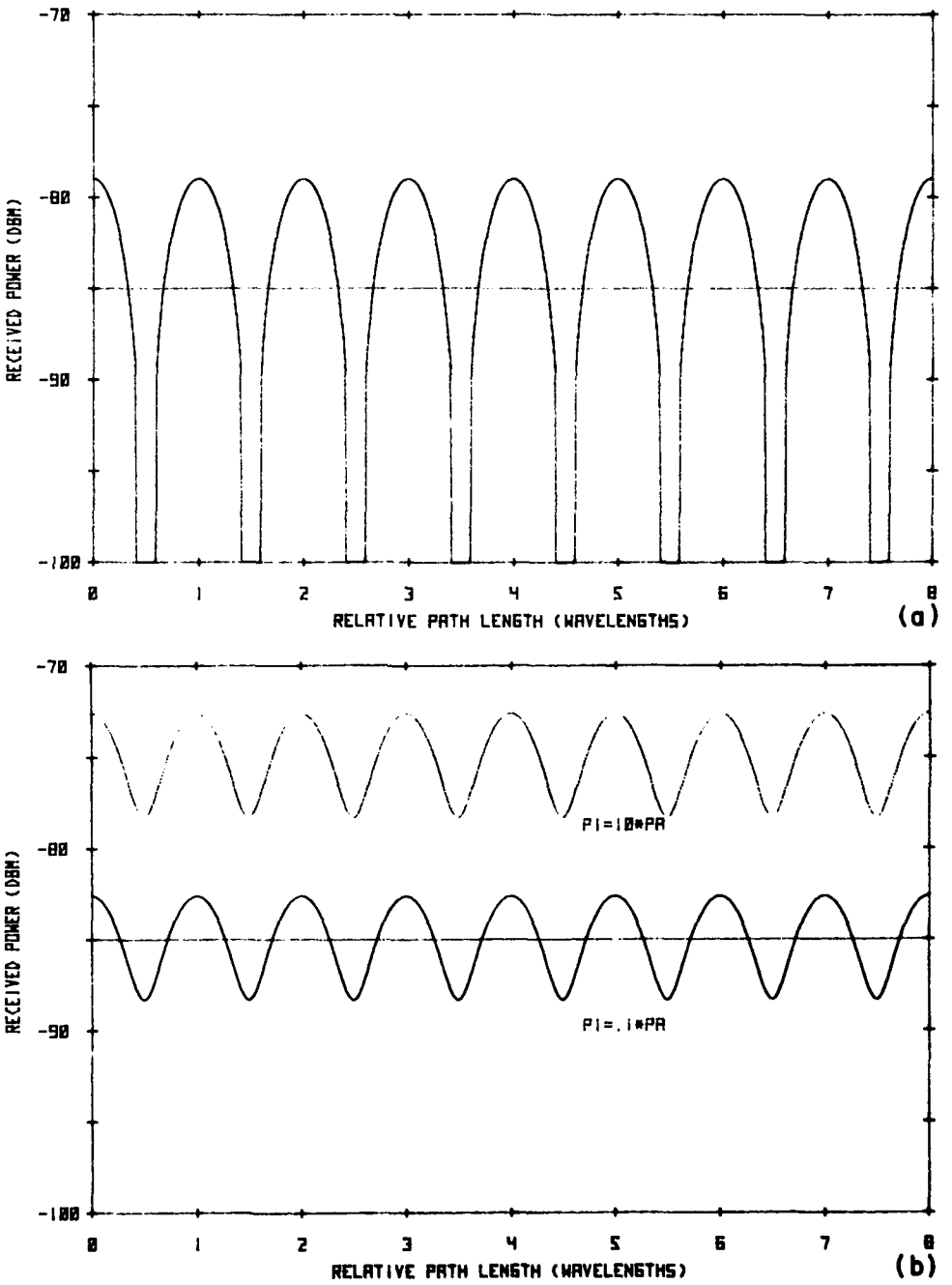

Figure 12. Amplitude of Received Power Variation as a Function of Ambient Power Level. (a) $P_I = P_A$, (b) $P_I = 10\ P_A$ and $P_I = 0.1\ P_A$

Even though a system could in fact be implemented that operated by measuring the received power and produced an alarm when the received power changed by a certain amount, it is more appropriate for the previously-discussed reasons to construct a receiver with a detector whose output is proportional only to the intruder's presence. In this section, the performance of receivers with two types of detectors will be considered.

4.1 Envelope Detector

The total voltage at the terminals of the receiving antenna can be written as

$$V_T(t) = B\left[1 + \frac{|V_I| e^{j(\upsilon-\phi)}}{B}\right] e^{j(\omega t+\phi)} \quad . \tag{29}$$

The explicit time dependence has been reinserted as $e^{j\omega t}$ where $\omega = 2\pi f$ and $\upsilon = \upsilon(z, x)$ is the phase angle associated with V_I. Eq. (29) is now in the standard form of an amplitude modulated signal[14] with a modulation index m given by

$$m = \frac{|V_I|}{B} \quad . \tag{30}$$

An envelope detector like that shown in Figure 13 extracts the modulation and after low-pass filtering produces an output

$$M = d|V_I| \; e^{j(\upsilon-\phi)} \tag{31}$$

where d is the gain constant associated with the detector. The magnitude of M is found to be

$$|M| = \frac{|A|d|v_o|\rho_o r_\rho}{\rho r}\left\{e^{-2\alpha_1 z} + 2|C_2| e^{(-\alpha_1-\alpha_2)z}\cos[(\beta_1 - \beta_2)z + \zeta] + |C_2|^2 e^{-2\alpha_2 z}\right\}^{1/2} \quad . \tag{32}$$

---

14. Carlson, B.A. (1975) Communications Systems, An Introduction to Signals and Noise in Electrical Communications, 2nd ed., McGraw-Hill Co., New York.

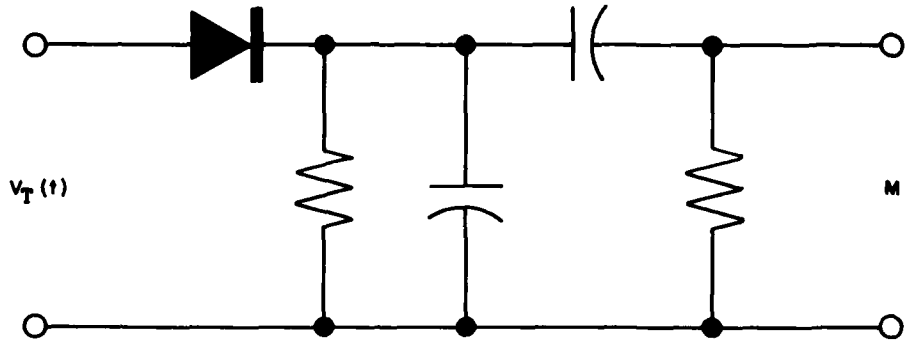

Figure 13. Sketch of Simple Envelope Detector

The phase of the message is similarly found to be

$$v = \alpha - \beta_3(r - r_o) + \delta + k' \tag{33}$$

where

$$k' = \tan^{-1}\left\{\frac{-\left[e^{-\alpha_1 z}\sin\beta_1 z + |C_2|\, e^{-\alpha_2 z}\sin(\beta_2 z - \zeta)\right]}{e^{-\alpha_1 z}\cos\beta_1 z + |C_2|\, e^{-\alpha_2 z}\cos(\beta_2 z - \zeta)}\right\}. \tag{34}$$

Thus an envelope detector produces an output signal which is independent of the ambient power level of the system. For convenience, $|M|$ is normalized to its value at $z = 0$, $r = r_o$, $\zeta = 0$, and $\rho = \rho_o$. The normalization factor is from Eq. (32) found to be $N = |A|d|v_o|(1 + 2|C_2| + |C_2|^2)^{1/2}$, and the normalized value of M is designated by M_E. The normalized response of the envelope detector is plotted in Figure 14 for a circumferential and a radial path. Inspection of the outputs show them to have the same general features of the curves previously shown. The fast oscillations are related to the coaxial wave mode velocity, and the slower ones resulting from the interaction of the coaxial and surface waves are evident. However, the amplitude of these variations now depends only on the intruder's signal strength.

In a practical system, the detected signal would now be filtered to remove any variations not produced by human frame motion. The resulting signal would then serve as the input to a thresholding circuit designed to respond to a minimum amplitude variation at its input.

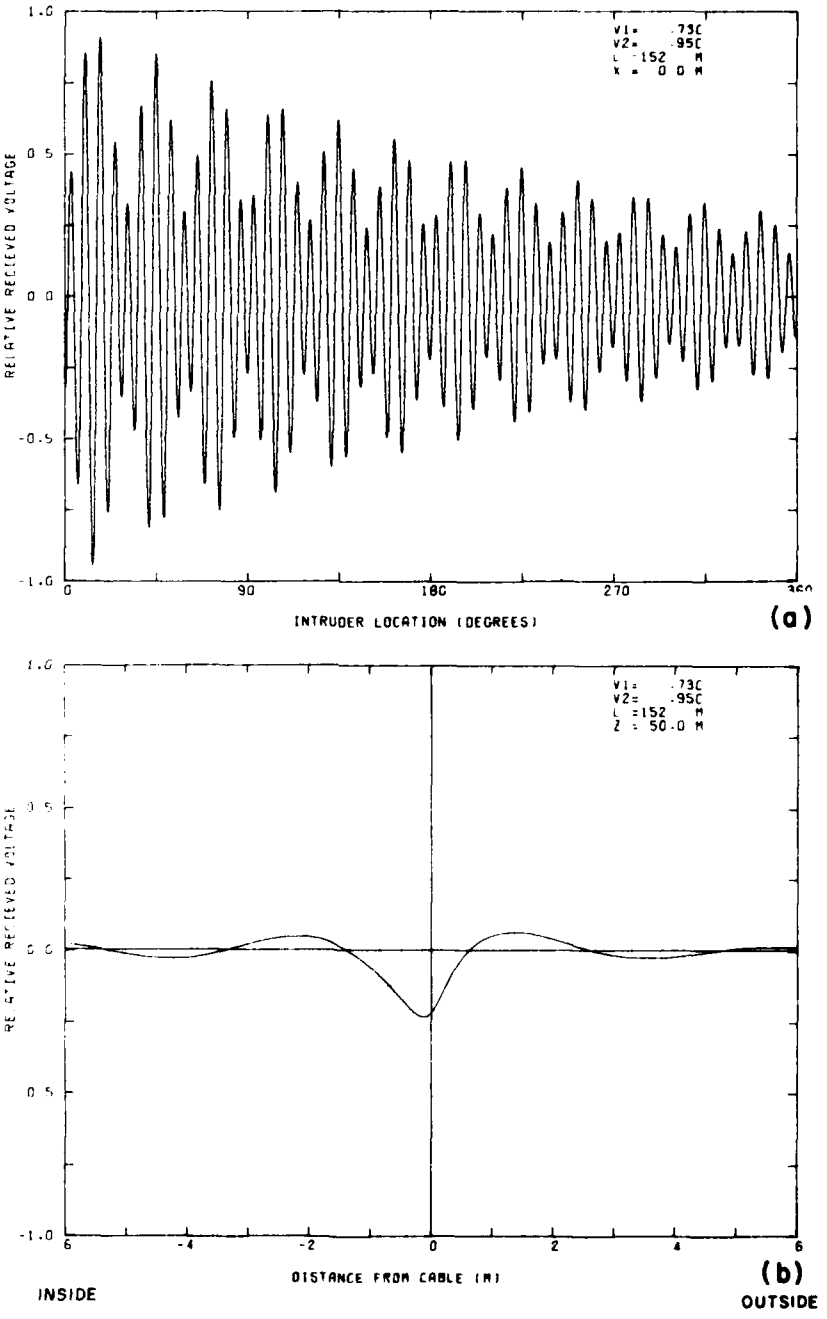

Figure 14. Response of Receiver with an Envelope Detector. $\gamma_1 = 0.0075 + j\,2.15\ m^{-1}$, $\gamma_2 = 0.01 + j\,1.65\ m^{-1}$, $y = 0.4$ m, $\xi = 0$ rad. (a) Circumferential Path, $\bar{X} = 0$ m, (b) Radial Path

4.2 Quadrature Detector

A block diagram of a basic quadrature detector is shown in Figure 15. The principal feature of such circuits is that they use two phase detectors which compare the phase of the received signal with two reference voltages that have a relative phase of $\pi/2$ radians. The output of the channel that uses the reference signal without the $\pi/2$ radian phase shift is the I signal. The reference signal for the other channel is shifted by 90° before being applied to the detector and its output is the Q signal. Thus, with the aid of Figure 15, the input voltage to each of the phase detectors is seen to be

$$V_T = \nu \left[B + |V_I| \, e^{j(\upsilon - \phi)} \right] e^{j(\omega t + \phi)} \quad . \tag{35}$$

The reference voltages are taken to be $R_I = \mu \, e^{j\omega t}$ and $R_Q = \mu \, e^{j(\pi/2 + \omega t)}$. Upon detection, the I and Q channel signals are found to be

$$I = d \, \mu \nu \left[B \, e^{j\phi} + |V_I| \, e^{j\upsilon} \right] \tag{36a}$$

and

$$Q = d \, \mu \nu \left[B \, e^{j(\phi - \pi/2)} + |V_I| \, e^{j(\upsilon - \pi/2)} \right] \tag{36b}$$

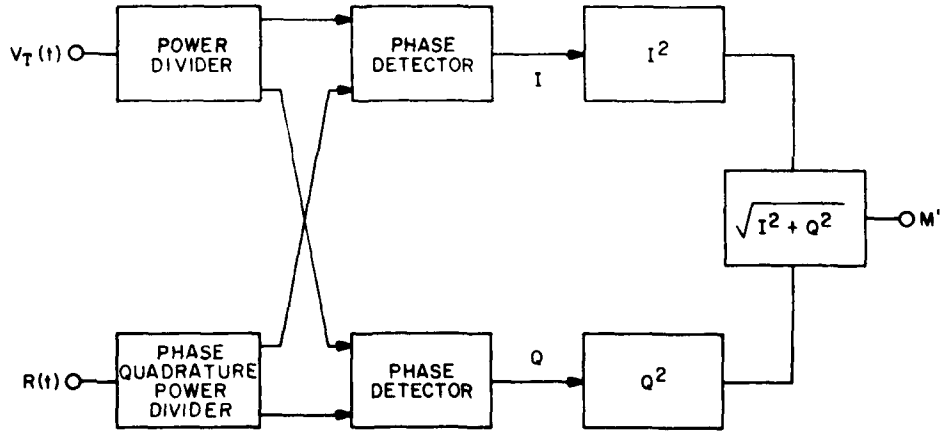

Figure 15. Sketch of Basic Quadrature Detector

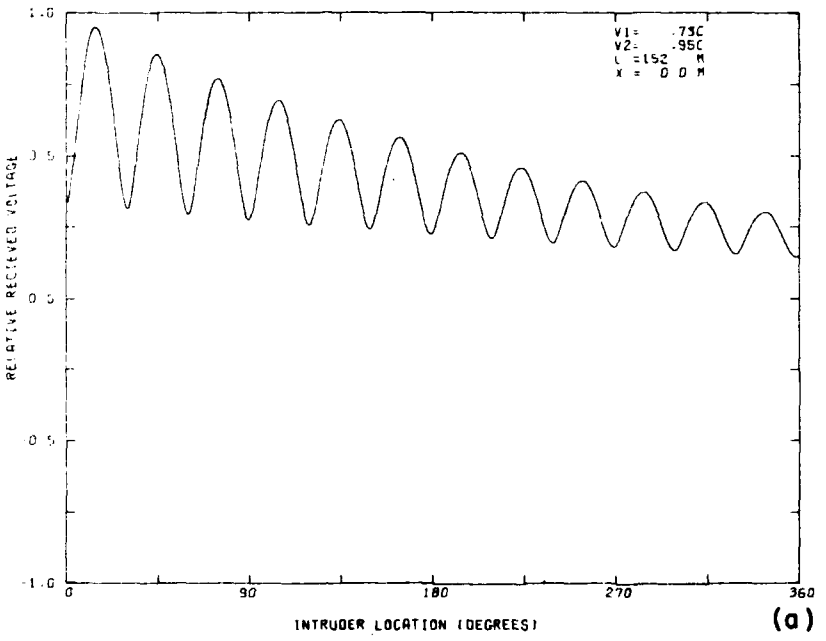

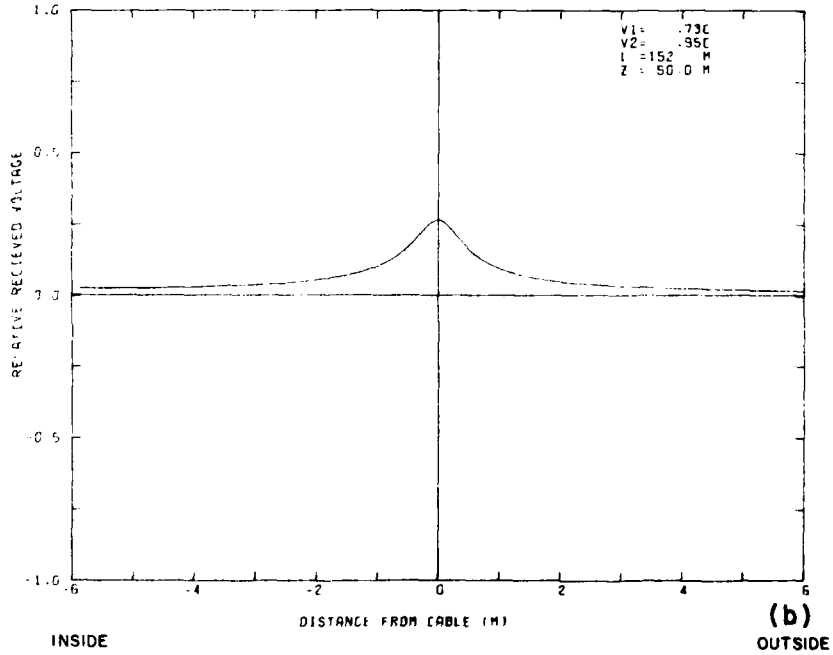

Figure 16. Response of a Receiver with a Quadrature Detector. $\gamma_1 = 0.0075 + j\ 2.15\ m^{-1}$, $\gamma_2 = 0.01 + j\ 1.65\ m^{-1}$, $y = 0.4$ m, $\xi = 0$ rad. (a) Circumferential Path, (b) Radial Path

respectively. After high pass filtering to remove the DC term produced by the ambient voltage, the two signals are squared and then added together. The square root of the sum is the quadrature detector output and is equal to

$$M' = \mu\nu|M| \quad . \tag{37}$$

Thus the output of a phase quadrature receiver is proportional to the magnitude of the output of an envelope detector. The normalized output signal, $M_{IQ} = M'/N$ where $N = \mu|A|d\nu|v_o|(1 + 2|C_2| \cos\zeta + |C_2|^2)^{1/2}$, is shown in Figure 16 for both a circumferential and a radial path. It is seen that for an I-Q detector, the output signal follows the envelope of the output of the envelope detector.

5. DETECTION SENSITIVITY

In this section, methods will be developed which can be used to estimate the performance of a single wire intruder detection system.

5.1 *Probability of Detection*

The probability of detection P_d for an intrusion detection sensor can be defined as

$$P_D(T) = \lim_{N \to \infty} \frac{n(T)}{N} \tag{38}$$

where n is equal to the number of crossings which produced an output signal equal to or greater than a threshold T out of the total number of crossings N. This definition requires that the intrusion paths be uniformly distributed and randomly selected.

It should be noted that the definition for P_D given by Eq. (38) is independent of the noise level of the receiver (false alarm rate) that is normally associated with the probability of detection[15] of radar systems. The reason for this is that the thresholds used in intrusion detectors greatly exceed the system noise levels. This is required to avoid nuisance alarms from small animals or other sources that would degrade the usefulness and user confidence in such systems.

Another feature which distinguishes intruder detection systems of this type from conventional radars is that the sensor field-intruder interaction occurs in the near field of the sensor. Thus the concept of target radar cross section,[16] a

15. Skolnik, M.J. (1962) Introduction to Radar Systems, McGraw-Hill Co., New York.

16. Skolnik, M.J., Editor (1970) Radar Handbook, McGraw-Hill Co., New York.

plane wave interaction model, does not apply. In general, the fields in the region where a detection would be expected are very nonuniform over the extent (height) of the intruder; this makes computation of the response extremely difficult. Instead, the P_D vs threshold curve is determined experimentally or computed using empirical data as will be done here for a particular target (intruder). The effect of intruder size and orientation is then estimated by adjusting the relative size of the scattering amplitude contained in the factor A.

Equations (31) and (37) can be used to generate curves from which $P_d(T)$ can be determined. This is done by randomly selecting a radial intrusion path and tabulating the maximum value of M_E and M_{IQ} for each path. The number of paths for which the output reached T compared to the total is for a sufficiently large N, the probability of detection for that threshold. The curves of P_D versus threshold are plotted in Figure 17 and can be used to estimate the performance of the system for various threshold settings. The greater overall sensitivity of the receiver with the quadrature detector is evident. It should also be mentioned that these P_D curves apply only to the sensor for which they were calculated. Changing a system variable such as the sensor length or cable attenuation results in a new P_D curve.

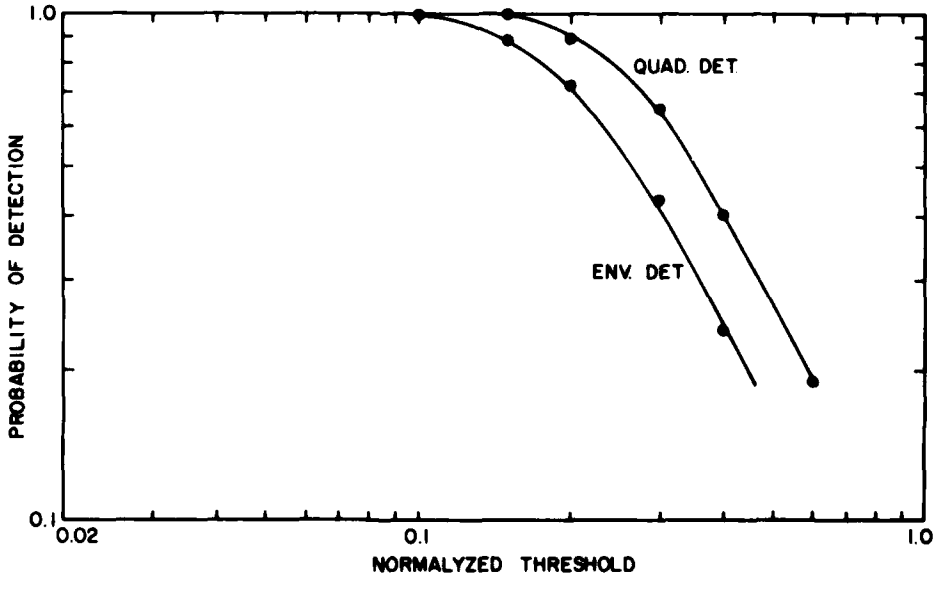

Figure 17. Probability of Detection as a Function of Threshold Voltage. $\gamma_1 = 0.0075 + j\,2.15\ m^{-1}$, $\gamma_2 = 0.01 + j\,1.65\ m^{-1}$, y = 0.4 m. N = 500, $C_2 = -0.5$

5.2 Zone of Detection

An equally important property of any intrusion system is its zone of containment Z_C, defined as the extent of the region in which a detection can occur. The most important single feature of a system is that its false alarm rate be adequately small. Thus, a sensor whose detection zone is only loosely controlled, and extends over a large range of distances from the sensor cable, is subject to detecting passing vehicles or people in areas where no detections are intended to occur.

For SWIRPS, the variation in detection sensitivity along the sensor is due chiefly to the cable attenuation and the interaction of the surface and coaxial mode waves. Of course, the presence of a resource which can modify the receiving antenna gain function so that $A = A(z)$ will also effect the uniformity of the zone of containment. Nevertheless, it is instructive to examine the factors which control and distort the Z_C of a system.

The variation in sensitivity along the sensor is easily computed with Eqs. (31) and (37). M_E and M_{IQ} are obtained as a function of position along a radial. The intruder first approaches the sensor cable from outside the loop and then executes another walk along the same radial from inside the loop. The two values of x where the detector output first reaches the threshold value (obtained from Figure 17 for a particular probability of detection) define extent of the detection fields along that radial. The zone of containment of the sensor is built up from similar calculations for successive radial paths. The results are plotted in Figure 18 for the envelope detector and the quadrature detector, respectively, for three values of P_D. It is evident in each of the six curves that the zone of containment extends farther away from the cable at the input end of the sensor than at the far end. Inspection of Figures 18(a)–18(c) shows that the number of areas where an intruder can reach or even cross the cable sensor without being detected increases as the threshold is increased. It is also clear that the overall efficacy of the system depends on setting the threshold low enough to obtain adequate detectability at the far end of the cable. Similar curves for a quadrature detector are shown in Figures 18(d)–18(f). They give a clearer picture of the zone of containment and its variation along the cable. A detection can only occur when an intruder is somewhere between the two curves of each figure. The regions where the two curves meet at the cable (x=0 m) represent those segments of the sensor where an intruder can pass undetected. As can be confirmed by examining Figure 18(d), 18(e), or 18(f), a P_D of 95 percent results in a sensor where 5 percent of the cable produces no detection. In practice, however, the small inhomogeneities in cable and ground properties make it impossible to predict the location of the insensitive zones, and setting the threshold somewhat lower can virtually eliminate them. However, the potential for false and nuisance alarm increases as the threshold is decreased, therefore a tradeoff of P_D vs nuisance or false alarm must ultimately be made.

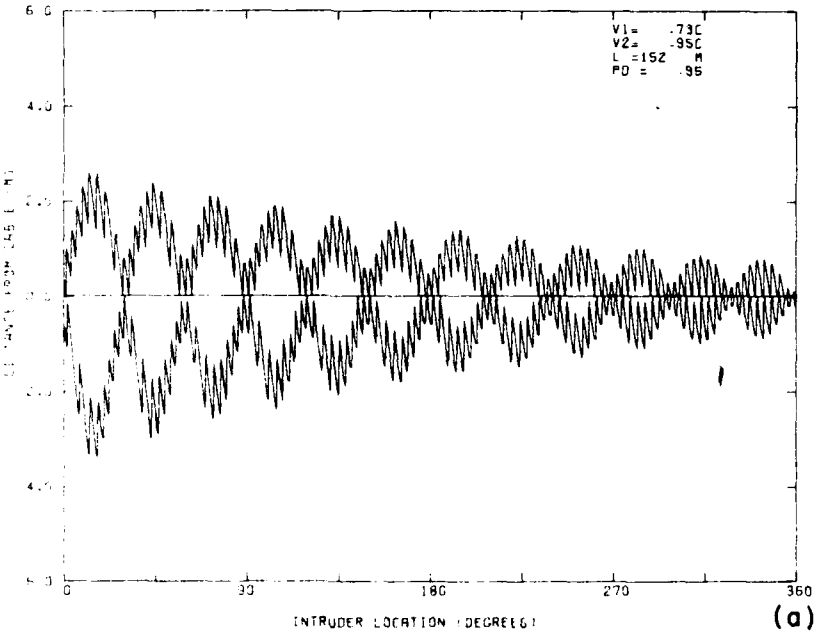

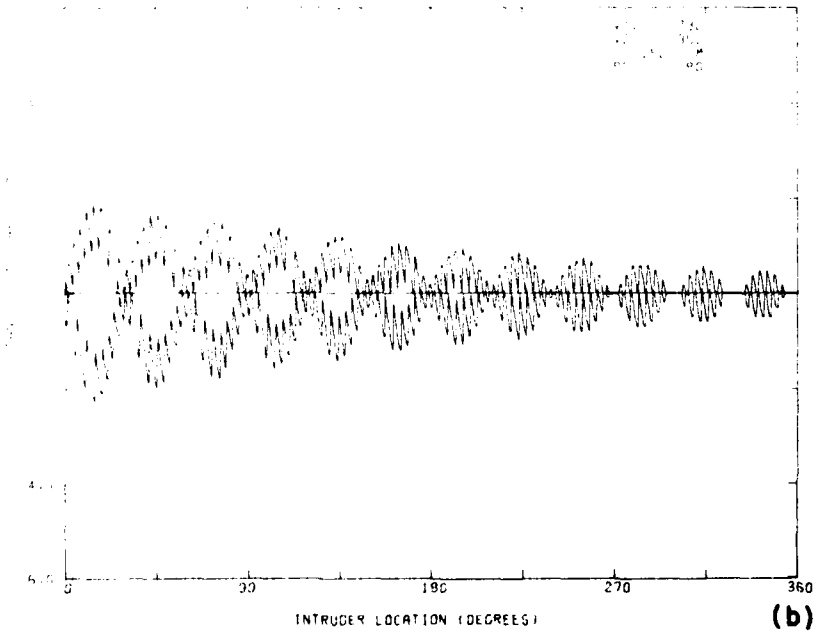

Figure 18. Zone of Containment. $\gamma_1 = 0.0075 + j\ 2.15\ m^{-1}$, $\gamma_2 = 0.01 + j\ 1.65\ m^{-1}$, y = 0.4 m. (a)–(c) Envelope Detector, (d)–(f) Quadrature Detector

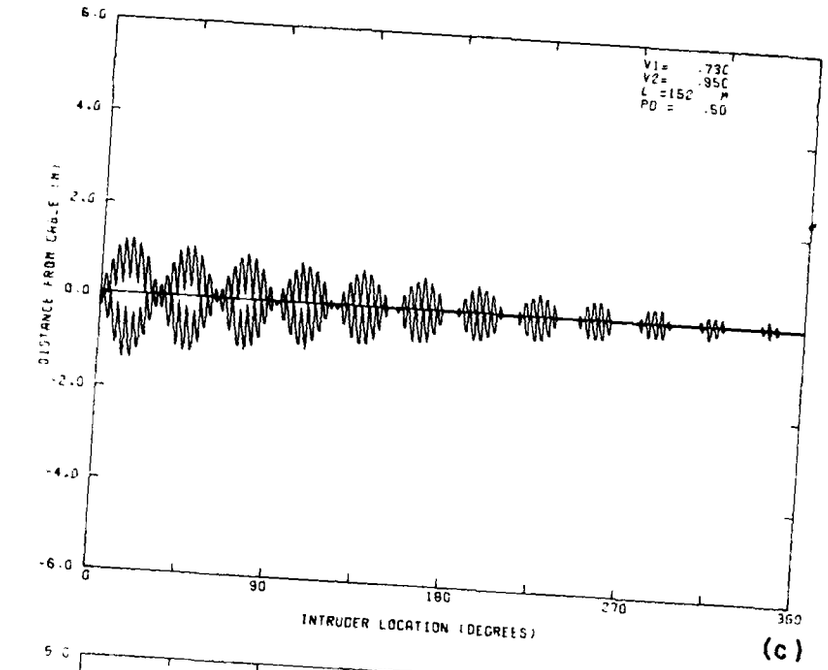

(c)

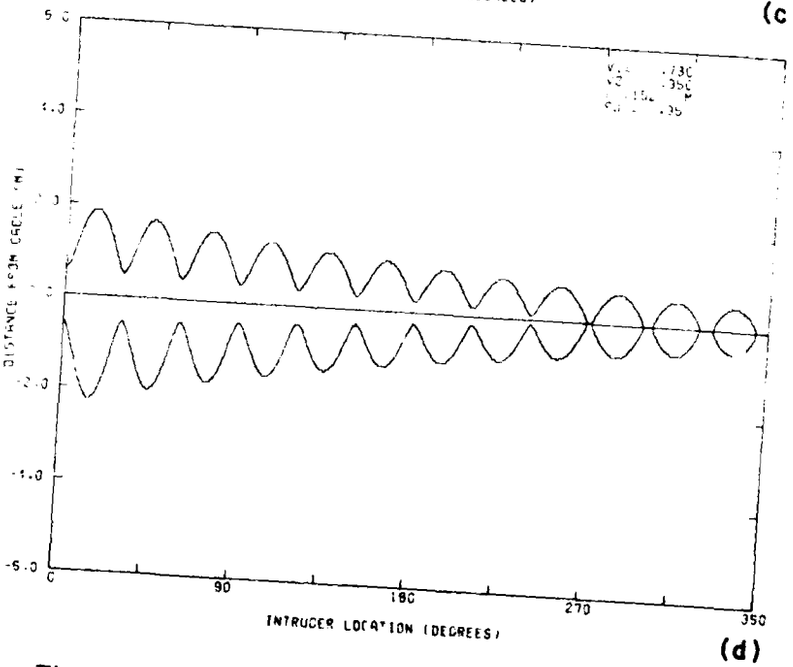

(d)

Figure 18. Zone of Containment. $\gamma_1 = 0.0075 + j\,2.15\ m^{-1}$, $\gamma_2 = 0.01 + j\,1.65\ m^{-1}$, $y = 0.4$ m. (a)–(c) Envelope Detector, (d)–(f) Quadrature Detector (Cont.)

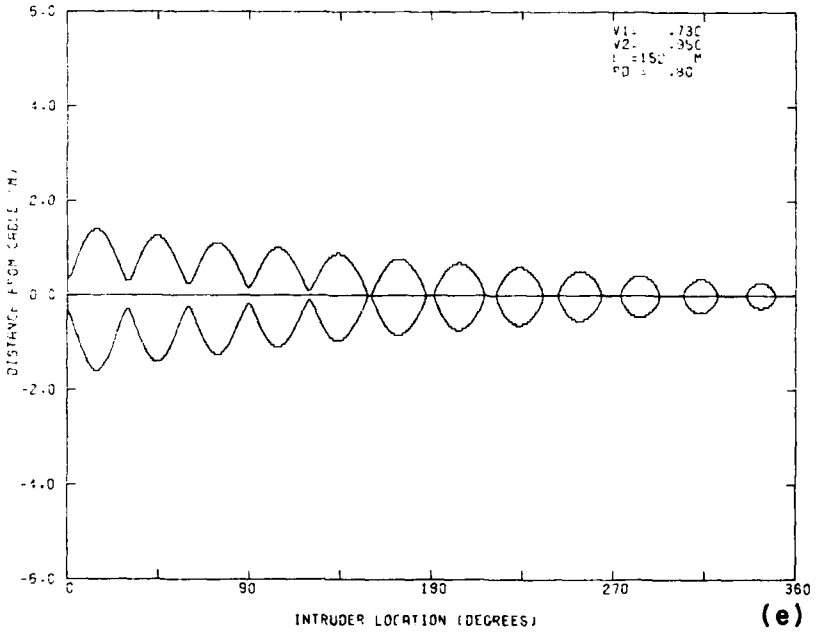

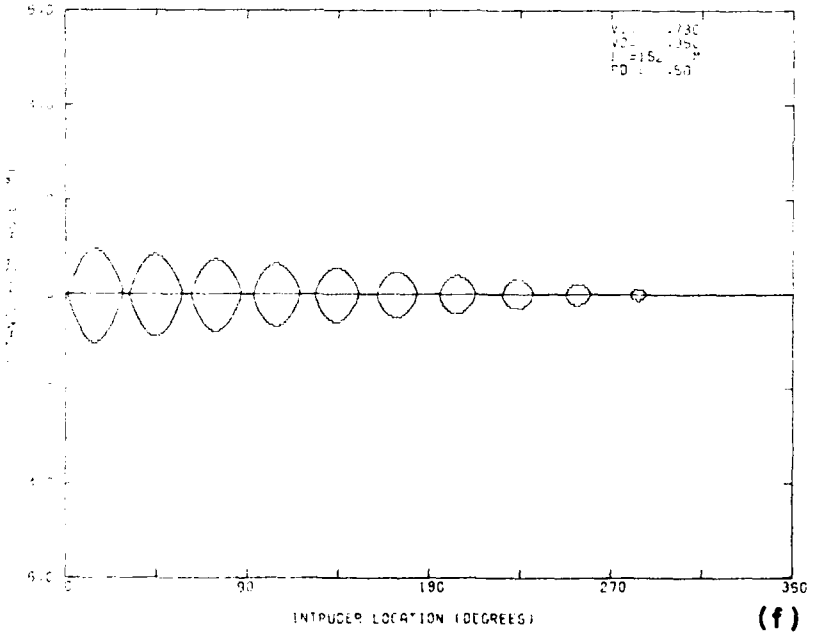

Figure 18. Zone of Containment. $\gamma_1 = 0.0075 + j\,2.15\ m^{-1}$, $\gamma_2 = 0.01 + j\,1.65\ m^{-1}$, y = 0.4 m. (a)–(c) Envelope Detector, (d)–(f) Quadrature Detector (Cont.)

The variation in the zone of containment with position discussed in connection with the curves in Figure 18 is an undesirable property of the sensor which becomes worse as the cable sensor length increases. The Z_C for the 350-m long sensor is shown in Figure 19. The gradual reduction in response is a consequence of α_1, which causes the signal propagating down the cable to be gradually attenuated, thereby reducing the power available at subsequent points along the sensor.

To diminish this effect, the cable must be designed to minimize α_1. Radiax[17] cables which are larger in diameter, of different construction, and not flexible compared to the CERT-285[13] used in these experiments do, however, have a smaller attenuation factor. The zone of containment computed for a system with such a cable is shown in Figure 20, and should be compared to that of the CERT cable in Figure 19. The improvement in uniformity of the Z_C along the sensor is evident. The P_D vs threshold is compared in Figure 21, where an improvement in system properties is also evident. The higher the allowable threshold for the same P_D, the lower the sensitivity of the system to false and nuisance alarms. Inspection of Figure 21 shows this trend for the less attenuative Radiax cable. From the results for Radiax cable, it can be seen that the most uniform detection characteristics would be achieved with a cable without attenuation.

The effect of zero attenuation, to produce a uniform detection zone, is achieved by increasing the size of the holes in the outer sheath of the leaky coaxial cable in proportion to the signal lost from attenuation and other sources. Determination of the proper rate of hole size increase is not easy since there is a strong interaction between cable attenuation, hole size (coupling coefficient), and the dielectric properties of the medium in which the cable is placed. However, if the cable is properly graded, the effect is to reduce α_1 to zero. Cables up to one-half mile long have been successfully graded and are used in an intrusion detection system called GUIDAR.[18] For the present purpose, the zone of detection for a system with a graded cable is computed by setting $\alpha_1 = 0$. The result is shown in Figure 22. The improvement in the uniformity of the response is clearly evident. The P_D curve of Figure 23 shows a further increase in the threshold required for obtaining a specified value of probability of detection.

In an actual system, the Z_C and P_D curves would show some random variation produced by differences in soil properties along the cable. Since the cable grading is carried out for typical operating conditions, it is also possible for the sensitivity of the sensor to increase with distance along the cable under certain favorable conditions, as, for example, when the ground is very dry or frozen.

---

17. Bulletin 1058A, Radiax Slotted Coaxial Cable, Andrew Corp., Orlando Park, IL.

18. GUIDAR Technical Brochure (1980) Computing Devices Co., Ottawa, Ontario, Canada.

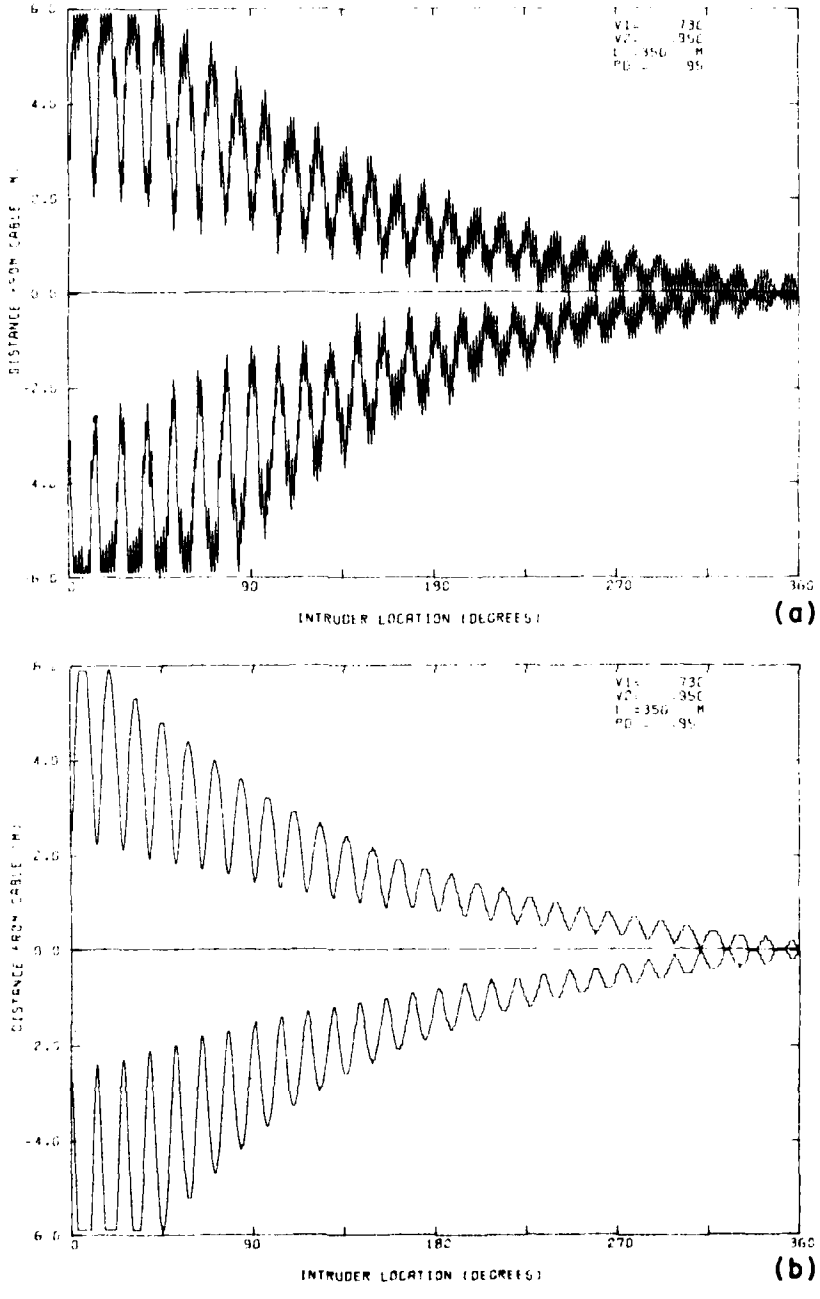

Figure 19. Computed Zone of Containment For a 350-m Cable. $\gamma_1 = 0.0075 + j\ 2.15\ m^{-1}$, $\gamma_2 = 0.01 + j\ 1.65\ m^{-1}$. (a) Envelope Detector, (b) Quadrature Detector

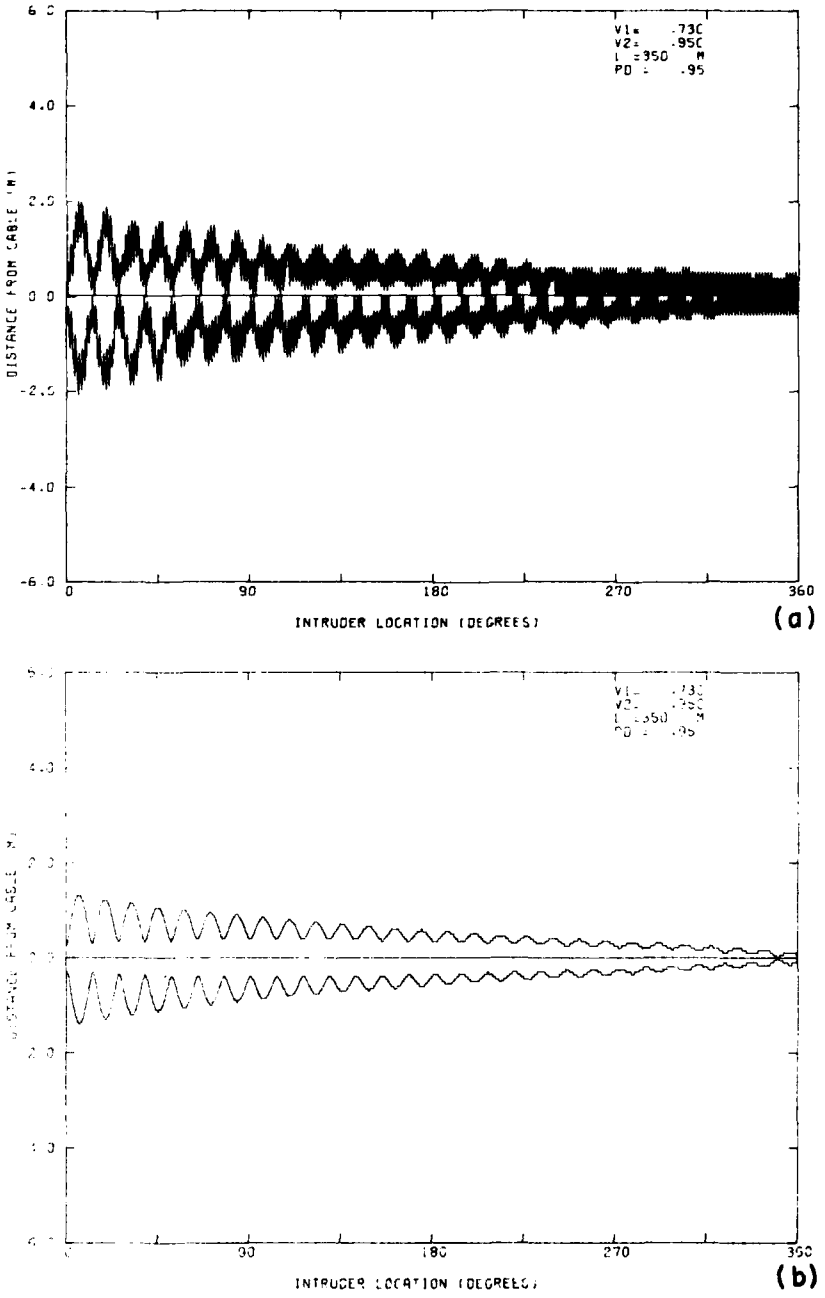

Figure 20. Zone of Containment Response For a 350-m Radiax Cable. $\gamma_1 = 0.0025 + j\,2.15\ m^{-1}$, $\gamma_2 = 0.01 + j\,1.7\ m^{-1}$, y = 0.4 m. (a) Envelope Detector, (b) Quadrature Detector

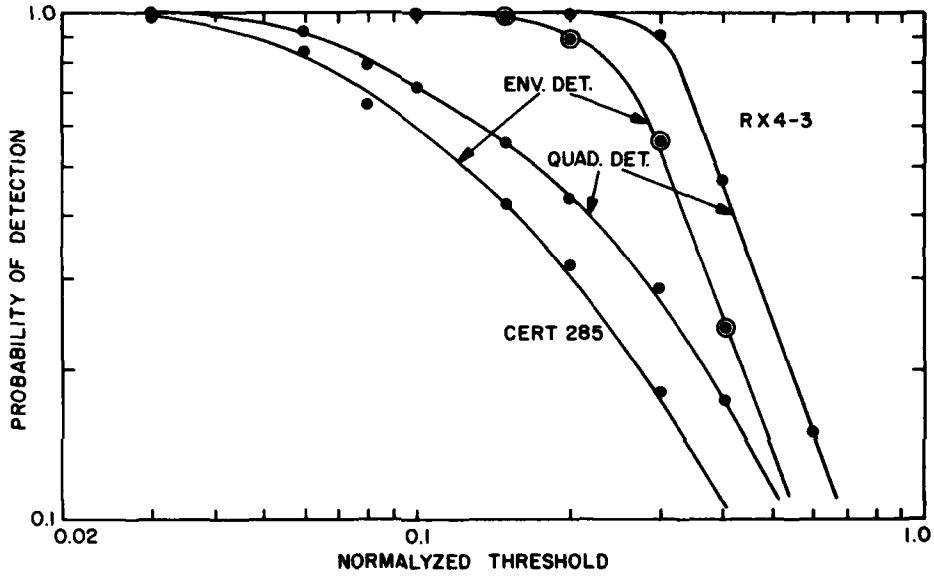

Figure 21. Comparison of the P_D vs Threshold for Two Cables. y = 0.4 m, L = 350 m, $\gamma_2 = 0.01 + j\ 1.65\ m^{-1}$. Radiax: $\gamma_1 = 0.0025 + j\ 2.15\ m^{-1}$, CERT: $\gamma_1 = 0.0076 + j\ 2.15\ m^{-1}$

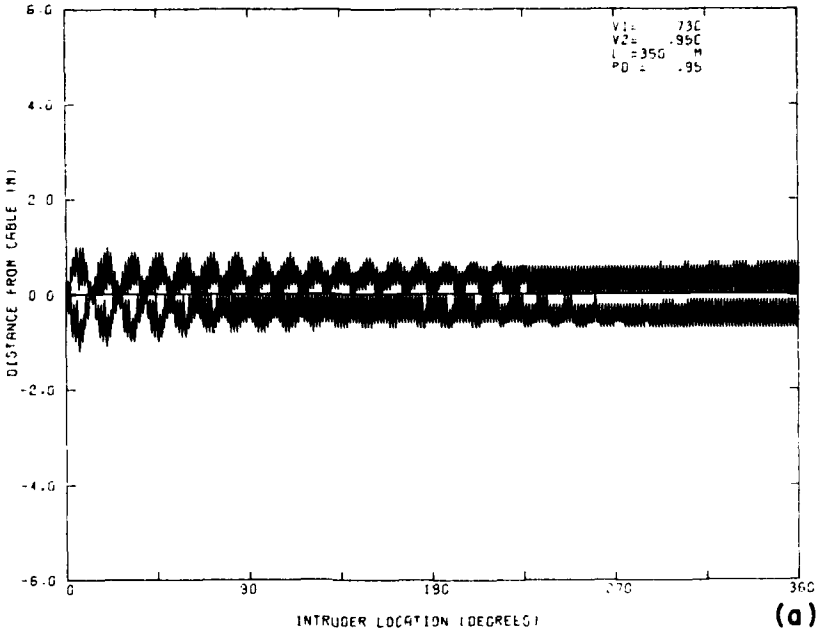

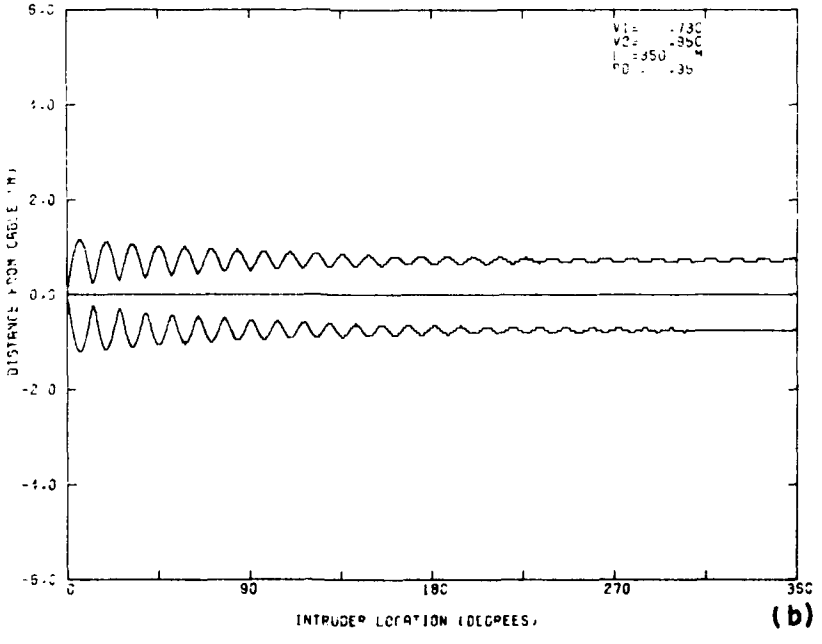

Figure 22. Zone of Containment for a Perfectly Graded Cable. $\gamma_1 = 0 + j\,2.15\ m^{-1}$, $\gamma_2 = 0.01 + j\,1.65\ m^{-1}$, y = 0.4 m. (a) Envelope Detector, (b) Quadrature Detector

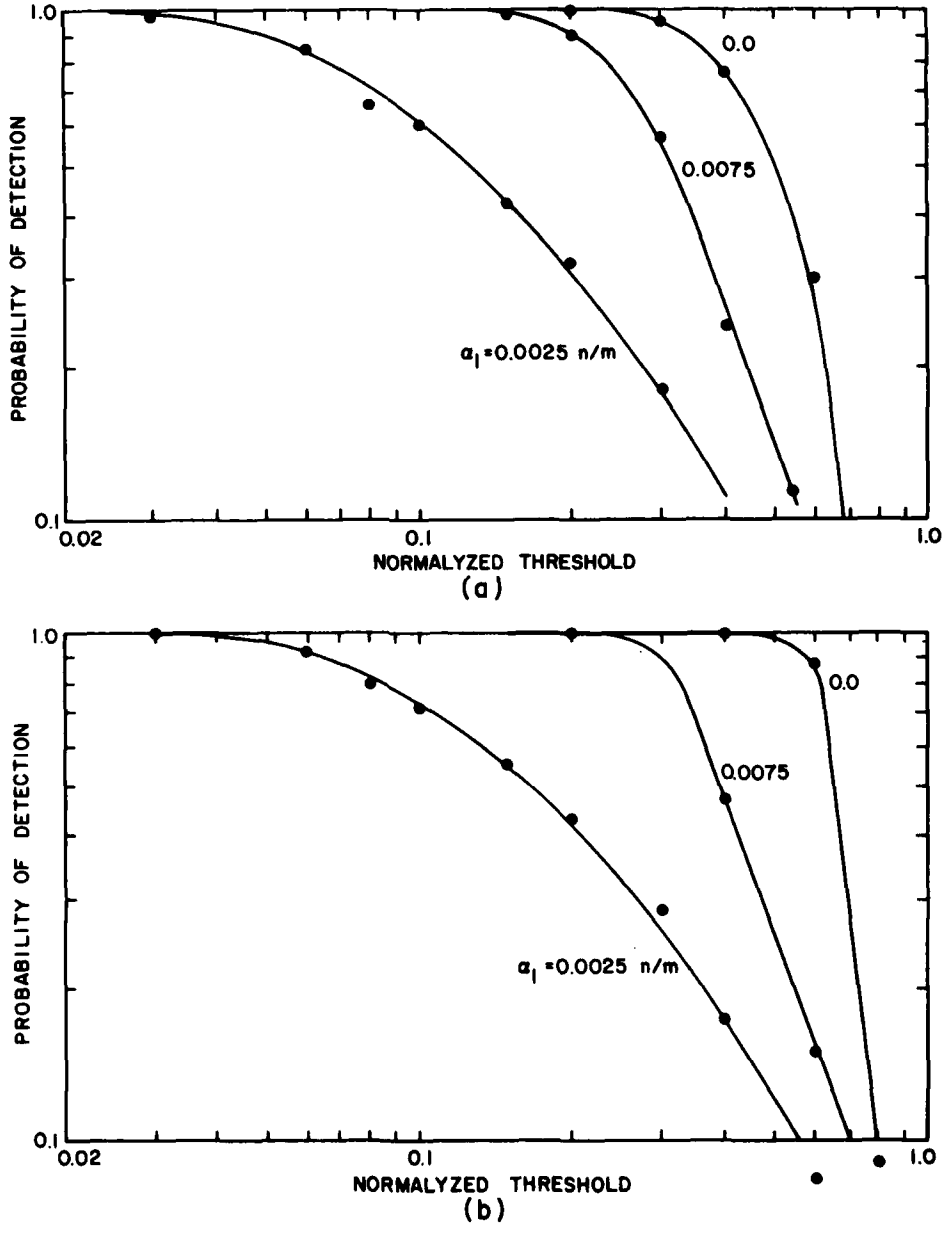

Figure 23. P_D vs Threshold for a Perfectly Graded Cable. $\gamma_1 = 0 + j\,2.15\ m^{-1}$, $\gamma_2 = 0.01 + j\,1.65\ m^{-1}$, y = 0.4, L = 350 m. (a) Envelope Detector, (b) Quadrature Detector

6. DISCUSSION

The preceding analysis focused on three aspects of the performance of an RF intrusion sensor. These were the radial decay of the field surrounding the leaky coaxial cable, the calculation of the probability of detection, and the computation of the zone of containment.

The radial falloff of the leaky cable field strength should follow a Hankle function law, although the initial 30 to 40 dB of the decay near the cable approximates a $1/\rho$ dependence. However, several workers have reported observing a $1/\rho$ dependence at distances beyond that predicted by the formal theory. The constant phase surfaces have been observed to be perpendicular to the cable. In view of this, a $1/\rho$ law is justified in many applications and was used in the calculations carried out here.

The theory for the Hankle function dependence of the fields presented in Barlow and Brown[10] can also be used to estimate the effect of changing the properties of the ground in applications where the cable is buried. The phase and amplitude of the radial decay depend on the dielectric constant and conductivity of the soil, as does the attenuation α_2. Generally, the transverse wave number increases with increasing complex dielectric constant, and causes the fields to decay more rapidly and the equiphase surfaces to tilt forward. Thus, for example, the decrease in the zone of containment of the sensor as a result of rain could be estimated.

The response of a system to intruders of different size can be estimated by computing the P_D vs threshold curve for different values of A. For example, measurements have shown that a crawling intruder produces a response about 6 dB lower than a upright person of identical size. Calculations of this type would allow the performance vs threshold to be computed for a broad range of expected targets.

The shape of the P_D vs threshold curve also provides information on the vulnerability of the system to false alarms. The higher the threshold can be set to reliably detect an intruder, the less the likelihood of a false alarm. A system false alarm is any alarm caused by the sensor, communication or display that does not result from a valid intrusion by personnel, ground vehicles, or nuisances. A goal of any system is to eliminate false alarms generated by internal noise and by natural and man-made environmental effects such as weather, electromagnetic radiation, and over-flying aircraft. A nuisance alarm is one generated at the sensor by any source that exhibits signatures similar to those of personnel, vehicles or other valid intruder. An example is the detection of small animals. The quality of the P_D vs threshold characteristic of a sensor is directly related to the uniformity of its detection properties along the sensor cable and the sensor's susceptibility to nuisance alarms.

Perhaps the most important aspect of system performance which was examined was the extent of the zone of detection and its uniformity. The principal factor affecting the uniformity of the Z_C is the attenuation of the cable which causes the sensitivity of the system to be greater at the beginning of the cable than at the end. Thus, if the overall sensitivity of the receiver is adjusted for reliable detection at the far end of the cable, then the system will be too sensitive near the input end and be vulnerable to false and nuisance detections. This undesirable behavior in performance is further accentuated as the attenuation and length of the cable increase.

The most direct way of eliminating the variation due to attenuation in the zone of detection is by grading the leaky coax cable. That is, the size of the holes along the cable are gradually increased in proportion to the reduction in signal from attenuation and other sources. This tends to keep the field strength outside the cable constant along the length of sensor, thereby resulting in a uniform zone of detection. The performance of a system with a perfectly graded cable can be evaluated by setting the attenuation factor α_1 equal to zero.

In summary, this report focused on the nature of the radial decay of the field around the leaky cable sensor, on the calculation of the probability of detection, and on the computation of the zone of containment. In contrast, two previous reports[1, 2] examined the response of similar systems in different configurations and with single and multiple receiving elements arbitrarily located within the sensor perimeter. The results of these allow the response of a leaky cable–antenna intrusion detection system in any configuration to be readily analyzed. The theoretical descriptions of the fields around the cable do not depend on the system configuration, and may be applied to a two-leaky cable system in which the receiving element is also a leaky cable.

References

1. Poirier, J.L. and Kushner, M. (1978) Analysis of the Response of an RF *Intruder Protection System*, RADC-TR-79-17, AD A072 816.
2. Poirier, J.L. (1979) Effects of Multiple Receiving Antennas on the Response of an RF Intrusion Sensor, RADC-TR-79-42, AD A072 819.
3. Rawat, V. (1973) Unorthodox Transmission Lines for Continuous Access Guided Communication (CAGC) PhD Thesis - Dept. of Electrical Eng., Queen's University, Kingston, Ontario, Canada.
4. Fernandes, A.S. de C. (1979) Propagation characteristics of a loose braid coaxial cable in free space, Radio and Electronic Eng., 49, No. 5, pp 255-260, May 1979.
5. Delogne, P.O. and Safak, M. (1975) Electromagnetic theory of the leaky coaxial cable, The Radio and Electronic Eng., 49, pp 233-40, May 1975.
6. Wait, J.R. and Hill, D.A. (1975) Propagation along a braided coaxial cable in a circular tunnel, IEEE Trans. on Microwave Theory and Techniques, MTT-23, No. 5, pp 401-5, May 1975.
7. Ambramowitz, M. (1964) Handbook of Mathematical Functions, N. Bur. of Stnd., U.S. Printing Office, Washington, D.C.
8. Cree, D.J. and Giles, L.J. (1975) Practical performance of radiating cables, REE, Vol. 45, pp 221-223, May 1975.
9. Yoh, P., Esposito, R., Gagnon, R., and Kodis, R.D. (1974) Measurements of Leaky Coaxial Cables and Possible Applications to Train Communications, Report No. FRA-ORD & D-74-43, U.S. Department of Transportation, May 1974.
10. Barlow, H.M. and Brown, J. (1962) Radio Surface Waves, International Monographs on Radio, Oxford at the Clarendon Press.
11. Harman, K. (1979) Private communication.
12. Poirier, J. Leon (1979) An Evaluation of Some Factors Affecting the Choice of Operating Frequency of a Guided Wave Radar for Intruder Detection, RADC-TR-79-83, AD A073 078.

PRECEDING PAGE BLANK-NOT FILMED